Journal of Volcanology and Geothermal Research 302 (2015) 33–46

Contents lists available at ScienceDirect

Journal of Volcanology and Geothermal Research

journal homepage: www.elsevier.com/locate/jvolgeores

Catastrophic flank collapses and slumping in Pico Island during the last 130 kyr (Pico-Faial ridge, Azores Triple Junction)

A.C.G. Costa [a,b,*], A. Hildenbrand [b,c], F.O. Marques [d], A.L.R. Sibrant [b,e], A. Santos de Campos [f]

[a] Universidade de Lisboa and IDL, Lisboa, Portugal
[b] Univ. Paris-Sud, Laboratoire GEOPS, UMR8148, Orsay, F-91405, France
[c] CNRS, Orsay, F-91405 France
[d] Universidade de Lisboa, Lisboa, Portugal
[e] Laboratoire FAST (CNRS/Univ. P-Sud), Orsay, F-91405, France
[f] EMEPC, Paço de Arcos, Portugal

ARTICLE INFO

Article history:
Received 25 November 2014
Accepted 10 June 2015
Available online 19 June 2015

Keywords:
Large-scale mass-wasting
Volcanic construction
Active slump
K-Ar dating
Pico Island
Azores Triple Junction

ABSTRACT

The Pico Island constitutes the easternmost sub-aerial domain of a steep WNW-ESE volcanic ridge, which has developed within the Nubia-Eurasia diffuse plate boundary (Azores Triple Junction). The island comprises three volcanic systems, from older to younger: the Topo Volcano, the Fissural System, and the Pico Stratovolcano. From a high-resolution Digital Elevation Model (10 m), and new bathymetric, stratigraphic, structural, and high-precision K-Ar data, we reconstruct the main successive stages of growth and partial destruction of the island over the last 200 kyr. We especially concentrate on the central sector of the island, which has recorded gradual movements through slumping and catastrophic flank collapses since ca. 130 kyr. The remmants of the Topo Volcano are partly exposed on Pico's SE flank, and are here dated between 186 ± 5 and 115 ± 4 ka. Topo was significantly destroyed by N- and S-directed large-scale flank collapses between ca. 125 and 70 ka. On Pico's N flank, collapse seems to have removed all the unstable material, but in the S the collapse structure is composite, including a major flank collapse and a remnant slump complex that is still active. A first episode of deformation occurred between ca. 125 and 115 ka along the master fault of the slump. Between ca. 115 and 69 ka, most of the unstable material was removed by a major flank collapse, leaving behind a still considerable volume of unstable material that comprises the active slump. This first collapse was catastrophic and generated a large debris deposit recognized on the high-resolution bathymetry, with a minimum run-out of ca. 17 km. The scar was partially filled by volcanic products erupted from volcanic cones developed within the slump depression, and possibly also from the early WNW-ESE Fissural System. Subsequent deformation in the slump area affected in part the filling units, leading to the individualization of secondary curved faults. Younger volcanic products have gradually masked the mass-wasting scars. Unlike the well-known Hilina slump (Hawaii), Pico's slump evolution might be controlled by an active regional tectonics.

1. Introduction

The evolution of oceanic islands is generally marked by the interplay between volcanic construction and repeated destruction by a variety of processes, from small (Ramalho et al., 2013 for the Azores) to large scale, including voluminous mass-wasting. Large-scale lateral flank instabilities have been recognized as a highly hazardous geological phenomenon documented around many volcanic islands worldwide, e.g. in Hawaii (Lipman et al., 1988; Moore et al., 1989, 1994; Moore and Clague, 2002), in Cape Verde (e.g., Day et al., 1999; Masson et al., 2008), in French Polynesia (Clouard et al., 2001; Clouard and Bonneville, 2004; Hildenbrand et al., 2004, 2006), in Lesser Antilles (Boudon et al., 2007; Germa et al., 2011), and in the Canaries (e.g., Carracedo., 1994; Krastel et al., 2001; Masson et al., 2002). Two main types of movement are classically distinguished: slow and gradual rotational movement along a deep detachment, often referred to as "slump", and (2) catastrophic rupture of an island flank, yielding the sudden generation of voluminous debris-avalanches, which can trigger destructive tsunamis (Moore et al., 1989; Satake et al., 2002). A slump can be followed by a catastrophic failure, and both types can affect a given island (e.g., Lipman et al., 1988; Moore et al., 1989). The volume of individual failure episodes partly depends on edifice size (Mitchell, 2003). The most extreme debris-avalanches have a run-out sometimes exceeding 100 km, and an individual volume up to several thousands of km^3. These giant deposits have been extensively recognized along

* Corresponding author at: Universidade de Lisboa and IDL, Lisboa, Portugal. Tel.: +351 918318361.
E-mail address: acgcosta@fc.ul.pt (A.C.G. Costa).

http://dx.doi.org/10.1016/j.jvolgeores.2015.06.008
0377-0273/

the Hawaiian Emperor volcanic chain, which comprises the largest volcanic islands on Earth (e.g. Moore et al., 1989, 1994). However, such episodes appear quite infrequent, with an estimated recurrence of about 100 kyr (Normark et al., 1993). In contrast, smaller volcanic islands seem to experience smaller but more frequent destabilization events, which still can amount to several km^3 and generate large tsunamis (e.g. Keating and McGuire, 2000). Therefore, studying lateral movements and repeated flank destabilization in relatively small volcanic islands like Pico is of particular scientific and societal relevance.

Pico Island is much smaller than most of the Canary or Hawaiian islands, but, in contrast, is located in an active tectonic setting. Like the other volcanic islands in the Central Azores, it is located on the diffuse boundary between the Eurasia (Eu) and Nubia (Nu) plates (Fig. 1A, e.g. Lourenço et al., 1998; Luis et al., 1998; Miranda et al., 1998; Fernandes et al., 2006; Borges et al., 2007; Lourenço, 2007; Hildenbrand et al., 2008; Luis and Miranda, 2008; Hipólito et al., 2013; Marques et al., 2013a, 2014a; Neves et al., 2013; Trippanera et al., 2013; Hildenbrand et al., 2014; Miranda et al., 2014), and sits on an anomalously elevated portion of the Mid-Atlantic Ridge (MAR, Fig. 1A) known as the eastern Azores Plateau. The inter-plate diffuse deformation is mostly accommodated by several extensional structures in a ca. 100 km wide area: (1) the Terceira Rift (TR, Fig. 1), and (2) the ca. WNW-ESE graben-horst-graben structure to the SW of the TR (Fig. 1B), which comprises the 200 m deep S. Jorge Graben (Lourenço, 2007) and the Faial Half-Graben, with an intervening horst, the S. Jorge/Faial Horst (Marques et al., 2013a, 2014a).

While the S. Jorge volcanic ridge developed apparently inside a graben, the Pico-Faial ridge developed in great part on the master fault bounding the north of the Faial half-graben (Fig. 1B). The sub-aerial growth of this ridge started ca. 850 ka ago on the eastern part of Faial Island (Fig. 1, Hildenbrand et al., 2012a), which has evolved through short periods of voluminous volcanic construction intercalated with longer periods of major destruction by both tectonics and relatively large-scale mass-wasting (Hildenbrand et al., 2012a, 2012b).The evolution of these steep volcanic ridges appears intimately related to tectonic deformation, which may partly control the successive stages of volcanic growth and repeated episodes of destabilization, e.g., through large-scale graben development (Hildenbrand et al., 2012a), flank collapses (Woodhall, 1974; Madeira, 1998; Nunes, 1999; Mitchell, 2003; Mitchell et al., 2008; Costa et al., 2014), or large-scale slumping (Nunes, 1999; Hildenbrand et al., 2012b, 2013; Mitchell et al., 2012a, 2013).

Despite the relatively small volume of the Azorean islands, increasing evidence for large-scale catastrophic destruction in the form of lateral flank collapses has been accumulated (Marques et al., 2013b; Costa et al., 2014; Sibrant et al., 2014, 2015a, 2015b). Large-scale mass-wasting on Pico's N flank was interpreted by Costa et al. (2014)

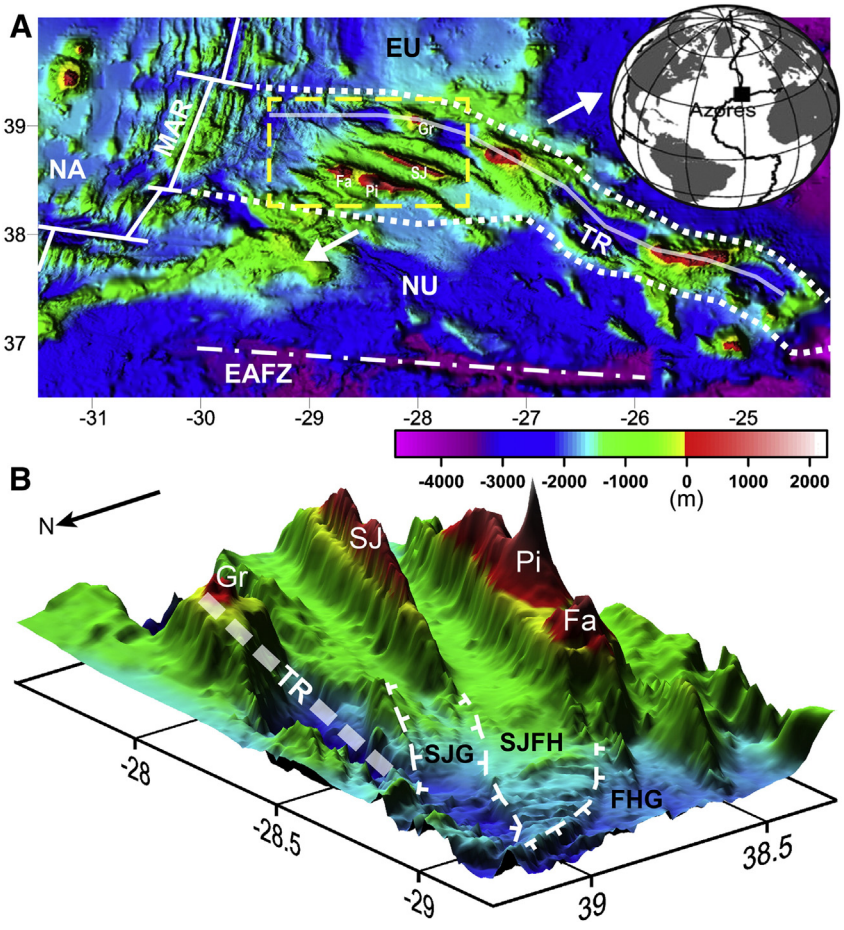

Fig. 1. (A) Location of the Azores archipelago on the diffuse boundary between the North America (NA), Eurasia (EU) and Nubia (NU) plates (lighting from WSW). Main active structures represented as: thick white line (Mid-Atlantic Ridge – MAR), thick semi-transparent white line (Terceira Rift – TR); limits of the diffuse Nu-Eu plate boundary represented by dotted lines and extension orientation indicated by thick white arrows; and inactive structure as dashed-dot-dashed white line (East Azores Fracture Zone – EAFZ). Yellow dashed rectangle marks the area presented in B. (B) 3D surface (viewed from NW and lighting from E, vertical exaggeration of approximately 10x) of the sector that includes the WNW-ESE Pico (Pi)-Faial (Fa) volcanic ridge studied in this paper. TR marked by thick dashed white line. The graben/horst structure SW of the TR is defined according to Marques et al. (2013a, 2014a). SJG – S. Jorge Graben; SJFH – S. Jorge/Faial Horst; FHG – Faial Half-Graben. SJ – S. Jorge Island; Gr – Graciosa Island. Bathymetric data from Lourenço et al. (1998).

as resulting from catastrophic collapse(s) towards the N. Pico's S flank is currently affected by an active large-scale slump with subsidence up to 1 cm/yr (Hildenbrand et al., 2012b), which comprises the western remnants of an earlier catastrophic collapse to the S. Though the current topography shows a well-defined scar extending much further to the E of the slump, which is suggestive of a flank collapse, there was until now no evidence of the catastrophic collapse, e.g. a debris deposit on the ocean bottom as recognized and described in the present work. Furthermore, the timing of initiation of the slump and the long-term interactions between gradual flank movement, catastrophic flank destabilization, volcanic activity and tectonics remain poorly constrained. Therefore, here we present the reconstruction of this sector of Pico Island, with special focus on the long-term evolution of the currently active large-scale slump that affects its SE flank (Hildenbrand et al., 2012b). We especially constrain with unprecedented temporal resolution the successive steps of evolution of the slump, and the occurrence of catastrophic flank collapse episodes.

The present study is based on the analysis and interpretation of high-resolution Digital Elevation Models (DEMs), detailed stratigraphic and structural observations and measurements, and high-precision K-Ar dating: (1) the geomorphological analysis from high-resolution sub-aerial and submarine DEMs allowed the interpretation of volcanic complexes, mass-wasting scars and offshore debris deposits; (2) the detailed stratigraphic observation along sea cliffs and creeks allowed the recognition of the main volcano-stratigraphic unconformities, and therefore to distinguish the main volcanic systems and their geometry; (3) the structural study, with the recognition and measurement of attitudes of faults, dykes and lava flows showed where the main structural discontinuities are, and their effects on the overall structure and evolution of the central part of the island; (4) the stratigraphic and structural data were used to carry out strategic sampling for K-Ar isotopic dating, which provides an accurate temporal framework to constrain the timing of volcanic construction and destruction episodes.

2. Geological background

2.1. Pico's morphology and volcanic stratigraphy

Pico is elongated WNW-ESE, with maximum length and width of ca. 46 km and ca. 16 km, respectively. It is part of the Faial-Pico volcanic ridge, which continues towards the SE as a submarine NW-SE trending ridge (e.g. Stretch et al., 2006; Lourenço, 2007; Mitchell et al., 2012b). The overall linear morphology of Pico Island is interrupted by two central-type volcanoes: the remnants of Topo Volcano, and the Pico Stratovolcano, which peaks at 2351 m above sea level (Fig. 2A). Strong slopes are locally observed over the island (Fig. 2B), mainly corresponding to: (1) coastal sectors where sub-vertical cliffs (maximum height of ca. 400 m on the northern flank) cut several volcanic successions, and (2) scarps related to mass-wasting/faulting, often masked by more recent volcanic deposits (Section 2.2). Previous studies have shown that Pico comprises three main volcanic complexes (Fig. 2A): (1) the relicts of an old extinct volcano in the SE, generally referred to as the Topo Volcano; (2) a linear chain of strombolian cones in the middle and eastern parts of the island, known as the Fissural System, which inflects from W-E in the E to WNW-ESE in the W near Topo Volcano (Nunes, 1999; França, 2000); the Fissural system becomes wider in the west, with a flatter top (<5–10°), towards the Pico Stratovolcano, where it is affected by the so-called Capitão Fault (*CF* in Fig. 2B, Madeira and Brum da Silveira, 2003); and (3) thePico Stratovolcano, which makes up the western half of the island (Fig. 2A). According to previous geochronological data, the sub-aerial part of Pico has developed during the last ca. 300 kyr (250 ± 40 ka, 270 ± 150 ka in Demande et al., 1982, Fig. 2A). Pico's sub-aerial growth seems to have started in the east, with the growth of the Topo Volcano (Fig. 2A, Zbyszewski et al., 1963; Forjaz, 1966; Woodhall, 1974; Madeira, 1998; Nunes, 1999; Nunes et al., 1999a), interpreted as a shield volcano by Woodhall (1974). Remnants of this early sub-aerial volcano have been unconformably covered by younger volcanic products poured from scattered scoria cones and WNW-ESE aligned cones making up the Fissural System (Zbyszewski et al., 1963; Woodhall, 1974; Madeira, 1998; Nunes, 1999; Nunes et al., 1999b, Fig. 2). The latest stages of island growth comprise the development of the Fissural System and the Pico Stratovolcano, which have been active through the Holocene, up to historical times (Fig. 2A, e.g., Zbyszewski et al., 1963; Forjaz, 1966; Woodhall, 1974; Madeira, 1998; Nunes, 1999; Nunes et al., 1999a.

Available K-Ar data on Pico are very scarce (Fig. 2A). A few whole rock K/Ar ages (Féraud et al., 1980; Demande et al., 1982) on samples from the three main units have been measured, but most of them are imprecise and overlap within the range of uncertainties, which can amount to more than 100 ka (cf. Fig. 2A). These ages, acquired on whole-rock samples, may also be significantly biased by the unsuitable incorporation of inherited excess ^{40}Ar trapped in phenocrysts (see Hildenbrand et al., 2012a). Therefore, none of them is useful to properly constrain the volcanic stratigraphy and the occurrence of destruction episodes (see also next section). A few radiocarbon data on charcoal fragments and/or paleosoils covered by lava flows help to constrain the age of some of the most recent eruptions (Madeira, 1998; Nunes, 1999). However, these data are also of limited use to study the long-term evolution of the central part of the island, due to the restricted applicability of the method (< ca. 50 kyr).

The lack of precise and representative isotopic ages in Pico (França, 2000), the lack of marked lithologic variability between main volcanic units (França, 2000; França et al., 2006), and the temporal partial overlap of volcanic activity, have hampered the definition of Pico's volcanic stratigraphy. The earlier works relied greatly on the published K-Ar and radiocarbon ages, on the alteration degree of the volcanic deposits, and on local field relationships (e.g., Madeira, 1998; Nunes, 1999; Nunes et al., 1999a; França, 2000; França et al., 2000), which is clearly insufficient for the objectives of the present work.

2.2. Mass-wasting in Pico Island

Earlier studies in Pico have highlighted the existence of several large structures affecting the various volcanic complexes (Fig. 2B): (1) two concave steep zones on Pico's northern flank (Fig. A.2a); (2) several nested scarps in SE Pico (Fig. 2C); and (3) a WNW-ESE scarp on the southern flank of the Pico Stratovolcano (Fig. A.2c). (1) On Pico's northern flank, a detailed analysis of high-resolution bathymetry and sub-aerial DEM, coupled with fieldwork and recent K-Ar dating on separated groundmass led Costa et al. (2014) to report a 4 to 10 km^3 submarine debris deposit, interpreted as resulting from a northwards catastrophic collapse on the N flank of the old Topo Volcano, prior to ca. 70 ka. and to report another flank collapse on the western sector Fissural system, prior to ca. 69 ka. (2) The easternmost scarp on the northern flank is mirrored in Pico's southern flank by another concave and steep main scarp and a series of less-pronounced scars (Fig. 2B and C). The westernmost scarp (Fig. 2) has been variably interpreted as: a crater or caldera (Zbyszewski et al., 1963), a "trap door" type caldera of Topo Volcano (Woodhall, 1974), a landslide scar (Madeira, 1998; Madeira and Brum da Silveira, 2003; Mitchell, 2003), or a fault constituting the headwall of a slump structure (Nunes, 1999, 2002; França, 2000; Hildenbrand et al., 2012b). Nunes (1999, 2002) proposed that this structure is younger than 37 ka and inactive since the beginning of the Holocene. This hypothesis was later reinforced by Mitchell et al. (2012a). These authors did not find evidence for current deformation of the island shelf by the slump structures, and considered that the lava delta was formed according to the present sea level. However, GPS data acquired between 2001 and 2006, and InSAR data acquired between 2006 and 2009, indicate

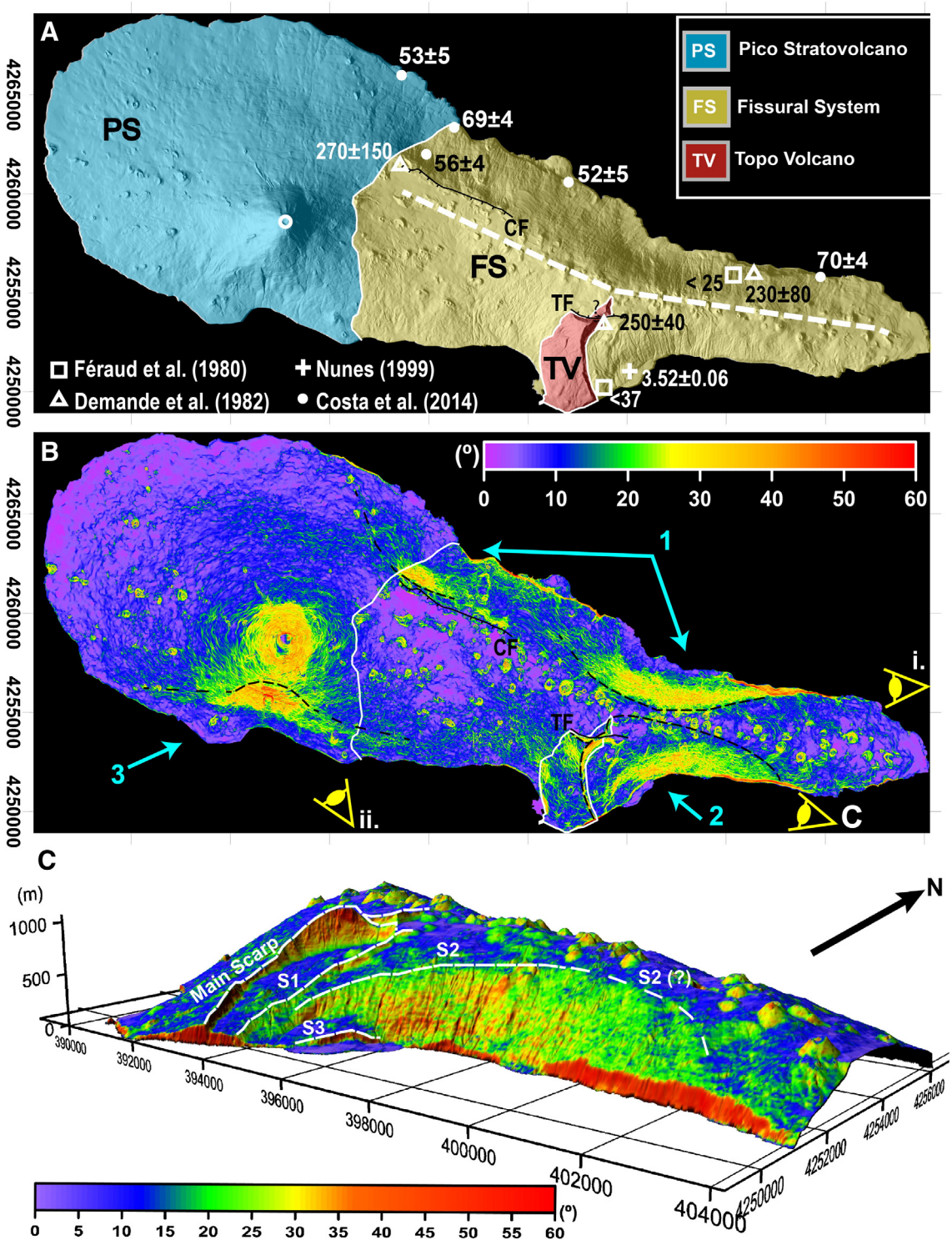

Fig. 2. (A) Shaded relief of the 10 m resolution DEM of Pico Island (lighting from WSW), with coordinates in metres UTM (zone 26N). White squares, triangles and circles mark the K-Ar ages from Féraud et al. (1980), Demande et al. (1982) and Costa et al. (2014), respectively. Also shown a radiocarbon age (plus sign) from Nunes (1999). The ages are indicated in thousands of years (ka). Simplified geologic/physiographic map (modified after Madeira, 1998). Traces of the Capitão Fault (CF) and Topo Fault (TF) (after Madeira, 1998; Nunes et al., 1999b; Madeira and Brum da Silveira, 2003). (B) Slope map of Pico Island built from the 10 m resolution DEM (additional details on the DEM construction are provided in Appendix A and in Costa et al., 2014). Dashed black lines: scarps interpreted from zones of anomalously steep slopes. The perspectives (yellow eyes) identified as *i*, and *ii* are presented as 3D surfaces in Figs. A.2a and A.2c, respectively (Supplementary Data – Appendix A). The perspective *C* is presented as a 3D surface in (C). (C) View from ESE of the slump structure's topography (lighting from SW). Image obtained by superimposing the 3D view of the slump relief (vertical exaggeration: 2x) and the slope map image (color scale indicated for slope angles), obtained from a 10 m resolution DEM. Scarps interpreted as white dashed lines (structures identification and interpretation modified after Hildenbrand et al., 2012b). The clean versions of these maps are presented as Figs. A.1 and A.2b.

that the slump structure is currently active, with horizontal displacement of 1.6 ± 1.3 mm/yr, and subsidence ranging between 5 and 12 mm/yr (Hildenbrand et al., 2012b, 2013). (3) The WNW-ESE scarp on the southern flank of the Pico Stratovolcano (Fig. 2B) has been interpreted either as an avalanche scar (Woodhall, 1974; Madeira, 1998; Madeira and Brum da Silveira, 2003) or as a fault

scarp (Forjaz, 1966; Machado et al., 1974; Chovelon, 1982; Forjaz et al., 1990; Nunes, 1999; Nunes et al., 1999a, 1999b; Mitchell, 2003). This scarp has been described as being masked by more recent volcanic products from the Pico Stratovolcano (Chovelon, 1982; Madeira, 1998; Nunes, 1999), and its base covered by recent and thick colluvium deposits (Madeira, 1998; Nunes, 1999).

3. Methods and results

3.1. Geomorphological analysis

A 10 m resolution sub-aerial DEM was complemented with bathymetric data acquired offshore Pico's SE flank (Figs. 2 to 5).

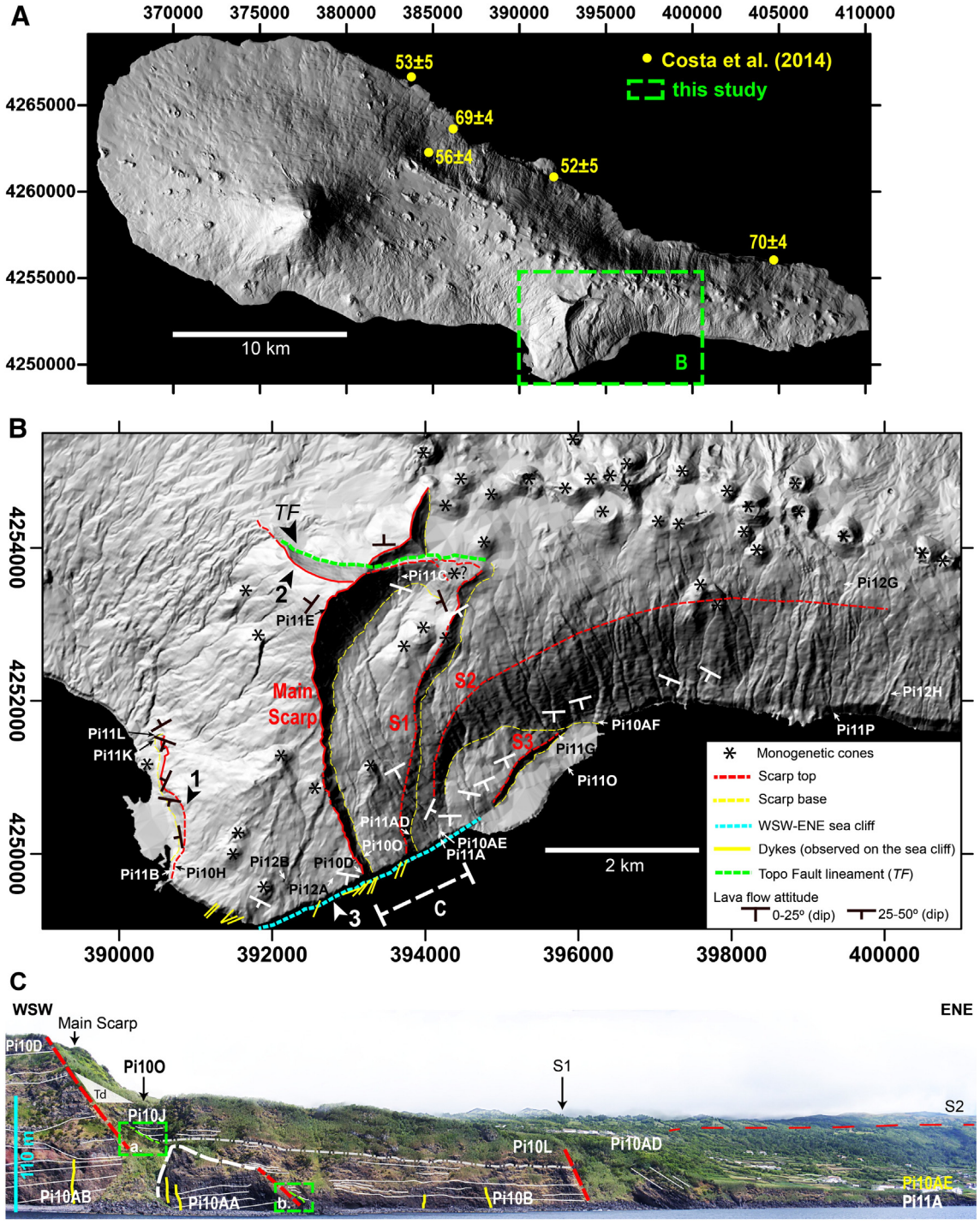

Fig. 3. Shaded relief maps (lighting from WSW in 3a., and from NW in 3b.), and image of the coastal section marked with *C* in 3b. (A) Ages from Costa et al. (2014) are shown in yellow, and the green dashed rectangle shows the sector on which we focused in this study. (B) Zoom of the slump sector, with indication of top and base of the scarps, identification of the scarps inside the slump area (after Hildenbrand et al., 2012b), indication of the attitude of lava flows, and location/identification of the new samples. The trace of the Topo Fault (TF) is shown as a green dash-dotted line. The sea cliff along which were performed the most relevant observations regarding the local stratigraphy is highlighted by a white dashed line labeled "C". The numbers show the main features addressed in text. (C) WSW-ESE view of the sea cliff marked as the *C* section (white dashed line) in Fig. 3B. Thin white lines – local orientation of the volcanic deposits as observed on the sea cliff. Grey dash-dotted line – possible unconformity. Red dashed lines – structural surfaces. Location/identification of the samples collected on (and in the proximities of) the sea cliff. Yellow lines – dykes. Green dashed rectangles *a* and *b* mark the zoomed images of the sedimentary deposits presented in Figs. A.3a and A.3b, respectively. *Td* – Recent talus deposit. A clean version of this figure is provided as Fig. A.4 (Appendix A). Zoom in figures of the sea cliff section are provided as Figs. A.5 and A.6 (Appendix A).

The submarine data include previously published data (Lourenço et al., 1998; Mitchell et al., 2012a) and new high-resolution bathymetric data with a spatial resolution between 50 m and 250 m, used here to identify potential debris deposits generated by catastrophic mass-wasting episodes in SE Pico. The topographic data were merged into a single grid. Details regarding data sources

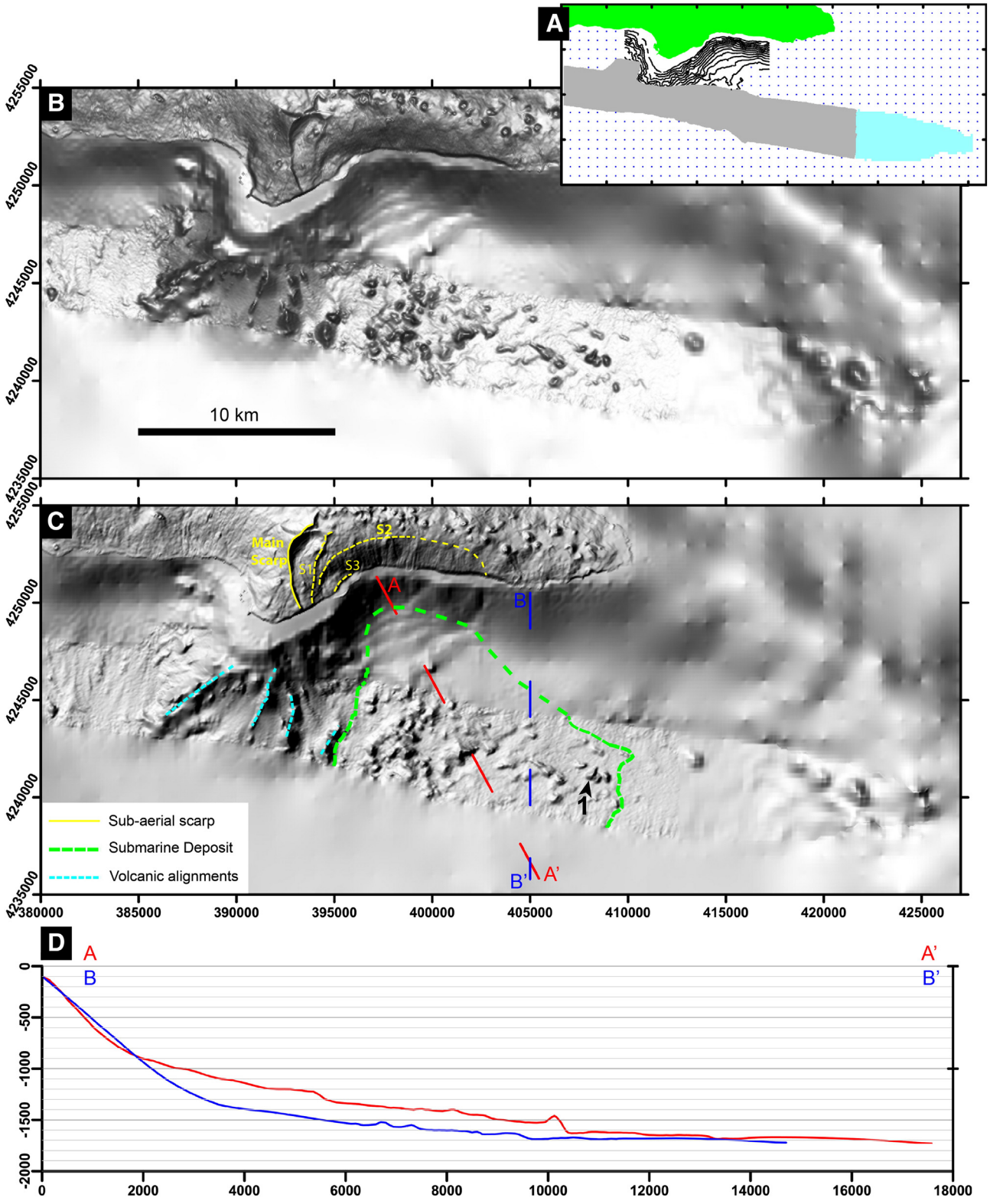

Fig. 4. (A) Different data sets used to compose the 50 m resolution grid presented in (B): green – 10 m resolution sub-aerial DEM; turquoise – 250 m resolution bathymetry; grey – 50 m resolution bathymetry; black lines – depth contours from Fig. 1B in Mitchell et al. (2012a); blue dots – bathymetric data extracted from the 1000 m resolution grid from Lourenço et al. (1998). (B) and (C) are shaded reliefs from the 50 m resolution grid, with vertical lighting and lighting from WNW, respectively. In C we interpreted the outline of the proximal sector of the hummocky terrain area (green dashed line), and the biggest block identified (*1*). We also indicate the alignments of submarine cones observed to the SW of Topo (light blue dashed lines), and the scars (yellow lines) identified in the sub-aerial sector adjacent to the submarine debris deposit. The apparent WSW-ENE lineaments visible in the area of interpolation of contours extracted from Mitchell et al. (2012a) constitute interpolation artefacts. (D) Topographic cross sections of the submarine flank indicated in (C). A clean version of this figure is provided as Fig. A.4.

and grid construction are provided in the supplementary material (Appendix A).

Shaded-relief and slope maps constructed from the synthetic grid allow the identification of important morphological features at both island and more local scales(Figs. 2 to 5, A.1, A.2, A.4 and A.7).

The remnants of the Topo Volcano are partly exposed in the central part of the island, where they constitute a prominent cape to the S of the axis of the Fissural System (Figs. 2A, 3A and B). They are partially masked by more recent volcanic products erupted from a SSW-NNE alignment of parasitic cones, which partially cover a small morphological scarp near the present sea level (*1* in Fig. 3B). The highest sector of Topo's preserved flank presents steep slopes up to 20–25° (Fig. 2B and C). There, the older volcanic sequence crops out, and the topographic surface truncates the volcanic sequence, suggesting that significant erosion has occurred. On the sub-aerial remnants of the Topo Volcano some main scarps can be recognized (Figs. 2C and 3B): (1) In the N, a N-facing scarp (*2* in Fig. 3B) that continues further E, and was interpreted by Madeira (1998) as the Topo Fault —*TF* in Fig. 3B). (2) In the SE, a 5 km-long prominent and straight WSW-ENE sea cliff (*3* in Fig. 3B, height up to 160 m a.s.l.), here interpreted as a fault. (3) In the E, the Main Scarp of the currently active slump (Fig. 3B, Hildenbrand et al., 2012b). It trends between NNW-SSE in the south and E-W in the north (where it affects both blocks of *TF*, Fig. 3B), and is thus concave to the SSE. Within the slump area, the Main Scarp and several smaller scarps are nested in one another, all concave to the SSE, which are designated S_n (Figs. 2C and 3B): S_1 presents a general SSW-NNE orientation, and its height and slope vanish towards the N. S_2 extends much further E than the area currently affected by the slump (as made clear in the slope map presented as Fig. 2C, and Hildenbrand et al., 2012b). Its trend is parallel to S_1 in the W (SSW-NNE), and parallel to the Fissural System axis in the east (E-W).S_3 trends SW-NE and vanishes towards the SW. Towards the NE, S_3 merges with S_2 (Figs. 2C and 3B). These collapse scarps are partially masked by deposits from monogenetic cones from the axial zone of the Fissural System and within the slump area, aligned along the slump scarps (Fig. 3B, monogenetic cones on the uppermost sector of S_1 and on S_2).

On the offshore of the slump area (Figs. 4 and 5), submarine alignments of small reliefs are interpreted as alignments of volcanic cones, with trends ranging from SSW-NNE to SW-NE (light blue dashed lines in Fig. 4C). The new high-resolution bathymetric data show a protuberant area of hummocky terrain extending up to, at least, 17 km from the coast, along the NW-SE direction, and reaching a minimum depth of ca. 1700 m (Figs. 4B to D, and 5). The large hummocks (largest hummock identified is ca. 850 m long – *1* in Fig. 4C) are significantly masked by smaller size material, especially in the domain closer to Pico's submarine slope (in agreement with Mitchell et al., 2012a, 2013). The imposed lighting in Fig. 4B and C highlight the irregular shape of these hummocks, here interpreted as large blocks.

3.2. Fieldwork and sampling

Our fieldwork investigations and sampling strategy were devised to constrain in time the main phases of volcanic growth and partial destruction of the central sector of Pico Island, more specifically in the southern sector (slump area). We concentrated our observations and sampling on the steep scarps, creeks, and along the high coastal cliffs where the exposure of the geological units is maximal. We performed stratigraphic and structural analysis in the field, and sampled for K-Ar dating the deposits at the base/top of the volcanic sequences separated by unconformities, especially the units cut by or sealing fault scarps. The strategy of sampling in the slump area is schematically shown in Fig. 6, and the exact location of the samples is presented in Fig. 3.

The preserved volcanic sequence of the Topo Volcano is partly exposed along scarp *1*, the WSW-ENE sea cliff (*3*), and *Main Scarp* (Fig. 3B). On scarp *1* (Fig. 4), we observed a basal sequence of lava flows gently dipping towards the W, unconformably overlain by lava flows and scoriae deposits (Figs. 3B and 6A). We sampled the basal sequence and a lava flow from the overlying sequence (Figs. 3B and 6A). Sea cliff *3* (Figs. 3B and C) comprises a succession of metre to decametre thick lava flows locally dipping towards the SW, and cut by sub-vertical dykes striking between N040° and N070° (Fig. 3B and C). We collected the lowermost accessible lava flows at the base of the sea cliff and the uppermost flows at the top of the scarp (Figs. 3B, C and 6A). In this sector, the Topo sequence is intruded by dykes near the Main scarp, and is locally affected by a recent rockslide deposit (Fig. 3C). To the E of the Main Scarp, we observed breccia/coarse talus deposits at mid-slope and near the seal level (*a* and *b* in Fig. 3C, respectively, with a zoom presented as Fig. A.3). The basal breccia deposit is overlain by a sequence of thin S-dipping lava flows (up to 1 m thick), which get thicker on the contact with the breccia (*b* in Fig. 3C), where a pahoehoe lava flow onlaps the basal topographic step of the Main Scarp (Fig. A.3b). Upwards, the mid-slope talus deposit is fossilized by generally massive lava flows (up to 10 m thick), which wedge out laterally against the main scarp (Fig. A.3a). Although we did not observe erosive truncation, the contrasting thickness of these

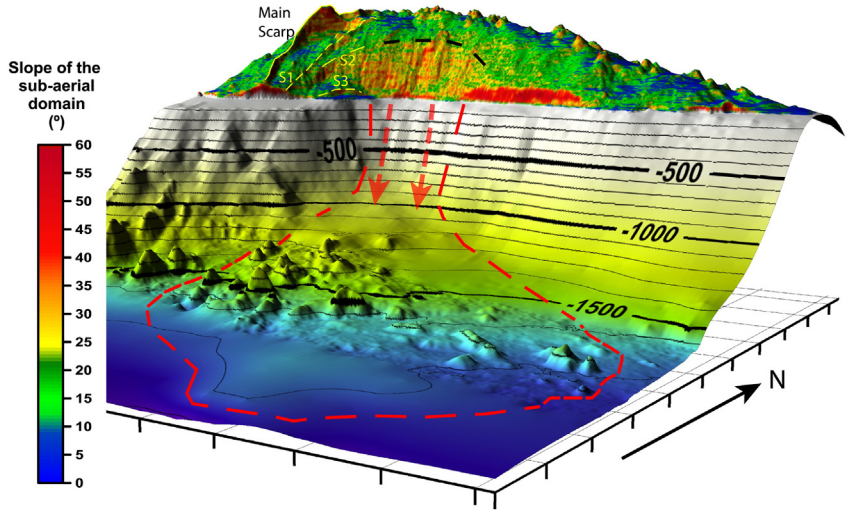

Fig. 5. 3D surface of the area represented in Fig. 4 viewed from SE, with elevation exaggerated 3x, and with lighting from SW. The sub-aerial domain is presented as a slope map. The extended outline and source of the deposit is interpreted with red dashed line and arrows. The interpreted sub-aerial source area for the debris material interpreted offshore is delimited by a black dashed line.

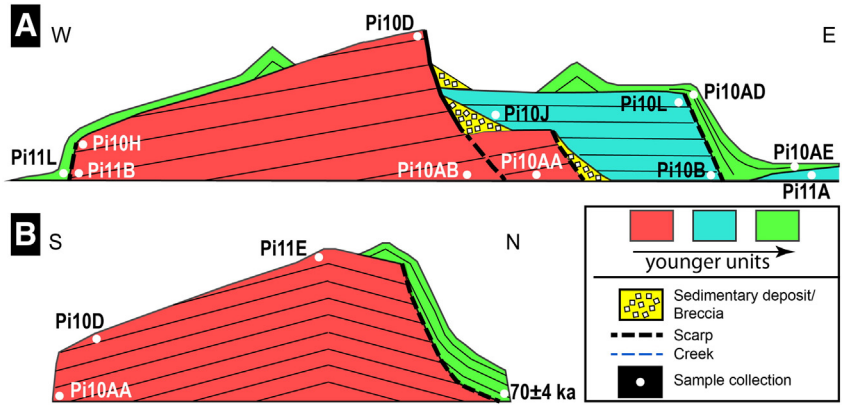

Fig. 6. Schematic illustration of the sampling strategy for (A) the Topo Complex/SE active slump (especially along the WSW-ENE sea cliff presented in Fig. 3C), and (B) the scars on the northern flank. The position of some of the key samples is shown as white dots (exact position presented in Fig. 3). The possible geometry of the northern flank follows the interpretation presented in Costa et al. (2014).

basal and upper lavas may constitute an unconformity (dash-dotted line in Fig. 3C, and Fig. A.6). This sequence to the E of the Main Scarp is cut by NNE-SSW-trending thin sub-vertical dykes. Further E, it is affected by the sharp S_1 (Fig. 3B and C). We sampled the lowermost and the uppermost lava flows of the sequence for dating purposes (Figs. 3C and 6A).

While S_1 is exposed on the sea cliff, inland it is masked by cascading lava flows, except on its topmost sector, where it cuts metre thick lava flows (Fig. 3B and C). East of S_1, the small sea cliff comprises a sequence of sub-horizontal lava flows intercalated with paleosoils (Fig. 3C). We sampled the basal and topmost lava flows of the coastal cliff at the foot of S_1, and a lava flow cascading over the scarp (Figs. 3C and 6A). Eastwards, along S_2, we only observed volcanic deposits (mostly lava flows) strongly dipping towards the sea (Fig. 3B). The eastern sector of S_3 comprises a monotonous sequence of metre thick lava flows, apparently corresponding to the lava flows that cascade over S_2 (Fig. 3B). On the western sector of S_3, the height and slope of the scarp decrease, and a sequence of thin cascading lava flows covers S_3, towards the current lava delta (Fig. 3B). We sampled a lava flow from the sequence exposed on S_3, and a lava flow from the lava delta (Figs. 3B and A.8). We also sampled the basal and topmost lava flows of the sequence cropping out on the sea cliff E of the slump area (easternmost samples in Fig. 3B).

3.3. K-Ar dating

We here present 24 new high-precision K-Ar ages (Fig. 7 and Table 1), which together with the 5 ages acquired by Costa et al. (2014) constitute an unprecedented dataset to reconstruct the main successive stages of growth and partial destruction of the island over its whole eruptive history. Our lava flow samples are fresh, aphyric to porphyric basalts (olivine, pyroxene and plagioclase phenocrysts), with low vesicular content. Dating precisely such young and mafic products requires the capability to measure extremely small amounts of radiogenic argon ($^{40}Ar^*$, in Table 1). The Cassignol-Gillot technique, developed at Lab. GEOPS (University Paris-Sud, Orsay) is particularly suitable for such purpose (Gillot et al., 2006). It allows dating young, even K-poor, volcanic rocks with uncertainties of only a few ka (e.g., Samper et al., 2007; Hildenbrand et al., 2008, 2012a; Germa et al., 2011; Boulesteix et al., 2012, 2013; Costa et al., 2014; Ricci et al., 2015).

The sample preparation included the following steps: (1) Careful observation of thin sections under a microscope to check that the samples have not suffered significant alteration; (2) crushing and sieving of the samples in order to obtain an homogeneous granulometry in the range 125–250 μm; (3) systematic removal of the phenocrysts through magnetic and heavy liquid sorting in order to extract the microlitic groundmass, which in the case of such basaltic samples is the only phase representative of the eruption age; (4) observation of the resulting sample under the binocular magnifier in order to attest its homogeneity. The groundmass samples obtained with this procedure present homogeneous size (125–250 μm) and density (2950–3050 kg/m^{3}for basaltic samples).

For each sample, K and Ar were both measured at least twice on distinct aliquotes of the homogeneous groundmass preparation by flame spectrophotometry and mass spectrometry, respectively. Details on the analytical procedure can be found elsewhere (Cassignol and Gillot, 1982; Gillot and Cornette, 1986; Gillot et al., 2006). The decay constants considered are from Steiger and Jäger (1977), and the age uncertainties are quoted at the 1σ level.

The volcanic sequence on the sea cliff cutting the Topo rocks was dated between 186 ± 5 ka and 125 ± 4 ka (Fig. 7). This old sequence is blanketed on the SW by younger volcanics erupted from parasitic cones, here dated between 60 ± 2 and 57 ± 2 ka.

Immediately east of the Main Scarp, the lava pile comprises ages between 115 ± 4 and 75 ± 4 ka (Fig. 7B). A lava flow sampled from the top of this sequence, at the foot of the Main Scarp, yields an age of 47 ± 3 ka (Fig. 7). S_1 is partially covered by a 49 ± 4 ka lava flow (Fig. 7B). The volcanic sequence at the foot of S_1 was dated between 90 ± 4 and 46 ± 4 ka (Fig. 7B). A lava flow cropping out on the eastern sector of S_3, and apparently cascading over S_2, was dated as 69 ± 4 ka (Fig. 7A). Towards the E, other lavas cascading over S_2 were dated between 43 ± 8 ka and 5 ± 3 ka. The lava flow that forms the eastern sector of the delta yields an age of 10 ± 2 ka (Fig. 7A).

The oldest ages determined for the northern slope of the Fissural System, published in Costa et al. (2014), correspond to the base of a prominent coastal cliff in the E, which was dated at 70 ± 4 ka, and to a lava flow masking an interpreted landslide scar in the W, which was dated at 69 ± 4 ka (Fig. 3A).

4. Discussion

4.1. Evolution of Pico's slump

The new K-Ar ages here presented, complemented by the data published in Costa et al. (2014), are fully consistent with our field observations, allow to reconstruct the step-by-step evolution of Pico's slump, and the occurrence of catastrophic flank collapses during the volcanic evolution of the island throughout the last 130 kyr. The new data especially show that the island has experienced several phases of rapid volcanic growth and episodic large-scale collapse(s).

The sub-aerial growth of the Topo Volcano is here constrained between ca. 186 ± 5 and 125 ± 4 or 115 ± 4 ka (Figs. 7 and 8). Given the present morphology of the Topo sector and the attitude of the lava flows (Fig. 7A), the summit of the Topo Volcano should have been

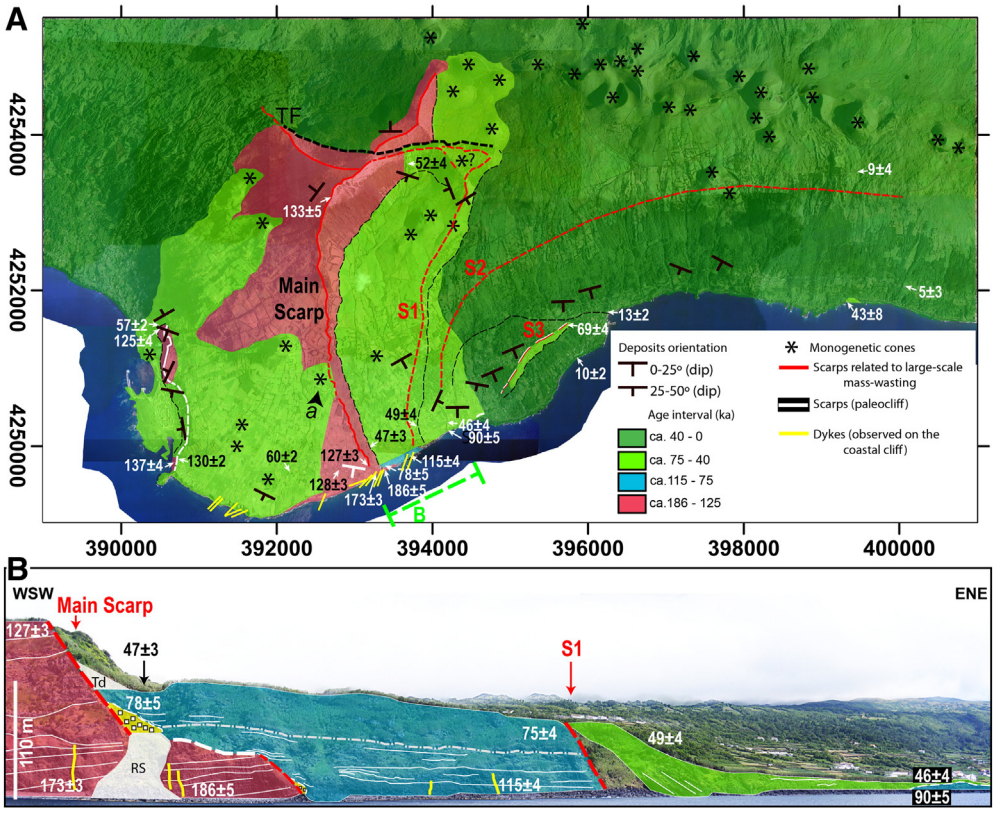

Fig. 7. (A) Geologic map built from the field observations and the new K-Ar data, with units defined as a function of the main unconformities observed in the field, and calibrated by the isotopic ages. Geology drawn on shaded relief with 10 m resolution DEM. (B) Interpreted profile of the coastal cliff indicated by green dashed line in (A). Grey dash-dotted line shows possible unconformity. Yellow lines represent dykes. *RS* corresponds to a recent small rockslide. *Td* corresponds to a recent talus deposit. Yellow wedge with embedded squares marks a talus deposit covered by the 78 ka lavas.

originally located in the topographic depression bounded by the Main Scarp, which is consistent with the positive gravity anomaly detected in this area (Nunes et al., 2006).

In the uppermost sector of the Topo volcano, the lateral contrast between the blocks to the S and N of the inferred Topo Fault (TF in Fig. 7A) support the existence of a fault that accommodated subsidence of the northern block (Madeira, 1998), but we could not find evidence for the strike-slip component proposed by Madeira (1998). Costa et al. (2014) suggested that the destruction of Topo's N flank involved gradual deformation along this structure, coupled with catastrophic failure towards the N more than ca. 70 ka ago. The youngest age of 125 ± 4 ka obtained for the Topo volcanic succession provides a new temporal bound, which now constrains the occurrence of the northern catastrophic flank collapse between ca. 125 and 70 ka.

In Pico's SE flank, in the currently active slump area, the collapse structure is much more complex than in Pico´s N flank, in terms of geometry, unconformities, faults, type of collapse, and ages. Most importantly, the collapse structure in the SE seems composite, i.e. with an earlier catastrophic collapse and a remnant still active slump, in great contrast to the northern collapses. Therefore, it deserves a more detailed discussion before coming to the conclusions.

At the shore level, there is an apparent discontinuity between sampling sites Pi10AA and Pi10AB (Fig. 3C) in the (downward) prolongation of the Main Scarp. This discontinuity can thus be interpreted as a fault segment (*Fault 1*, Fig. 8). However, the ages of the lava flows on the base of the sequences affected by this possible fault show an older age on the hanging wall (Fig. 7A), seemingly inconsistent with a normal fault. Given the concave shape of the Main Scarp, and that the lava flows dip to the SW, the ca. N-S part of the Main Scarp must have a dextral strike-slip component that can justify the ages obtained to each side of the fault (Fig. 8).

Some tens of meters farther east, the irregular discontinuity interpreted as *Fault 2* (Fig. 8) is apparently connected to the Main Scarp. *Fault 2* is overlain by old breccia/talus deposits, and it separates two volcanic sequences of distinct ages (ca. 186 – 127 in the foot wall, and ca. 115 – 75 ka in the hanging wall). The age of 115 ± 4 ka obtained for the base of the hanging wall sequence almost overlaps within the range of uncertainties with 125 ± 4 ka, the youngest age obtained for the Topo Volcano. Therefore, the lava flow here dated at ca. 115 ka may either constitute (1) the top of Topo Volcano edifice displaced by a (normal) fault, or (2) the base of a volcanic sequence filling a low topography created during an early phase of destruction of Topo Volcano (Fig. 8). (1) In the first hypothesis, gradual displacement along *Fault 2* would imply a cumulative vertical displacement of at least 200 m (current difference in altitude plus erosion of Topo's top) during a maximum period of 115 kyr, which gives an average conservative rate of ca 2 mm/yr. Such value is a minimum, because the lava flows onlapping the mid-slope talus deposit at the foot of the Main Scarp are here dated at ca. 78 ka. This suggests that significant movement on *Fault 2* occurred between ca. 115 ka and 78 ka, which would indicate an average rate of downward displacement closer to 5 mm/yr. Noticeably, the two rates here estimated are similar to present vertical displacements recorded by GPS and InSAR data within the SE Pico slump (Hildenbrand et al., 2012b). This scenario implies Topo's youngest sequence is presently under sea level, and without any unconformity separating the 125 from the 115 ka lavas. (2) In the second hypothesis, an early phase of destruction affected the Topo Volcano between ca. 125 and 115 ka (Fig. 8). A catastrophic collapse seems unlikely, because the submarine slopes offshore *Fault 2* seem globally preserved, though slightly disrupted (Fig. 4), and because if a catastrophic collapse had occurred between ca. 125 and 115 ka, the volcanic flank would have had to be reconstructed in this short time span (we dated a sub-aerial ca. 115 ka

Table 1
Results of the K-Ar dating in the present study. The ages are presented in thousands of years (ka). The results are reported at the 1σ level. For sample Pi11E, the two Ar analyses did not overlap at 1σ, and therefore the uncertainty on the mean ages is obtained from the standard deviation to the average.

Samples	UTM E	UTM N	K (%)	$^{40}Ar^{*}$ (%)	$^{40}Ar^{*}$ (10^{10} at/g)	Age (ka)	Uncertainty (ka)	Mean (ka)
Pi10AA	26393459	4249592	0.864	4.9	16.479	183	5	186 ± 5
				5.1	17.048	189	5	
Pi10AB	26393316	4249531	0.811	7.5	14.452	171	3	173 ± 3
				8.0	14.771	174	3	
Pi11B	26390763	4249755	1.042	3.7	14.619	134	4	137 ± 4
				3.5	15.303	141	5	
Pi11E	26392854	4253249	1.084	6.8	15.482	137	3	133 ± 5
				6.8	14.716	130	3	
Pi10H	26390851	4249857	1.227	8.6	16.832	131	2	130 ± 2
				8.2	16.589	129	2	
Pi12A	26392889	4249607	1.04	7.1	14.163	130	3	128 ± 3
				7.3	13.724	126	2	
Pi10D	26393271	4249709	1.223	4.8	15.951	125	3	127 ± 3
				5.3	16.440	129	3	
Pi11K	26390641	4251460	1.102	3.6	14.291	124	4	125 ± 4
				4.0	14.452	126	4	
Pi10B	26393790	4249778	1.029	3.7	12.375	115	3	115 ± 4
				3.6	12.437	116	4	
Pi11A	26394364	4250173	1.096	2.1	10.414	91	5	90 ± 5
				1.9	10.152	89	5	
Pi10J	26393403	4249657	2.025	1.7	16.183	77	5	78 ± 5
				1.4	16.646	79	6	
Pi10L	26393814	4249872	1.085	2.9	8.399	74	3	75 ± 4
				1.4	8.544	75	6	
Pi11G	26395876	4251479	0.717	1.7	5.247	70	4	69 ± 4
				1.9	5.153	69	4	
Pi12B	26392279	4249613	1.153	3.0	7.174	60	2	60 ± 2
				3.8	7.297	61	2	
Pi11L	26390641	4251460	1.074	2.4	6.587	59	3	57 ± 2
				2.6	6.251	56	2	
Pi11C	26393748	4253573	1.453	4.9	8.342	55	1	52 ± 4
				5.7	7.576	50	1	
Pi10AD	26394024	4250211	0.912	1.2	4.552	48	4	49 ± 4
				1.7	4.693	49	3	
Pi10AE	26394268	4250217	0.942	1.1	4.715	48	4	46 ± 4
				1.1	4.283	44	4	
Pi10O	26393298	4249923	1.12	1.3	5.862	50	4	47 ± 3
				2.1	5.267	45	2	
Pi11P	26399484	4251796	1.067	0.6	4.830	43	8	43 ± 8
				0.5	4.794	43	9	
Pi10AF	26396362	4251625	1.077	0.7	1.481	13	2	13 ± 2
				0.5	1.309	12	2	
Pi11O	26395881	4251008	1.278	0.4	0.951	7	2	10 ± 2
				0.5	1.651	12	3	
Pi12G	26399372	4253385	1.109	0.1	0.687	6	5	9 ± 4
				0.3	1.199	10	4	
Pi12H	26400154	4251895	1.15	0.1	0.208	2	3	5 ± 3
				0.2	0.691	6	3	

lava flow). Therefore, we prefer the hypothesis of a gradual downward movement of the island flank close to the Main Scarp. The subsided sequence of Topo would be presently under sea level, with an unconformity separating the 125 from the 115 ka lavas. The short time-span between the age of affected and filling units also means that initiation of the slump between 125 ka and 115 ka was followed by significant volcanism filling part of the former SE depression at ca. 115 ka. This supports a significant eruptive response to flank movement, as observed on other oceanic islands (e.g., Manconi et al., 2009; Boulesteix et al., 2012). However, in Pico's case, early slumping was not followed by the growth of a large, well-individualized post-collapse edifice. The attitude and the dip of the 115 ka lava flows filling the depression could suggest that they were erupted from small cones located on the headwall zone, but these feeders have not been found.

The ca.115–75 ka volcanic sequence is bounded in the E by a steep S_1, which is partly covered by a cascading lava flow equivalent to our sample Pi10AD, here dated at 49 ± 4 ka (Fig. 7B). This suggests that S_1 accommodated significant deformation between ca. 75 and 49 ka (Fig. 8). The lava flow sampled at the base of S_1's hanging wall is here dated at 90 ± 5 ka, which is very close to the age of one of the uppermost lavas from the ca. 115–75 ka succession (sample Pi10J, age of 78 ± 5 ka), within the range of uncertainties (Fig. 8). This suggests that, like the Main Scarp, S_1 developed in a gradual rather than catastrophic way. Consequently, we infer that, locally, the displaced flank of the old volcano is under the present sea level, immediately at the foot of S_1 (Fig. 8).

In contrast, the submarine flank of the island is clearly interrupted by a large embayment offshore S_2 (Fig. 4), and the debris field recognized on the distal submarine slope closely matches the sub-aerial extension of S_2 (Fig. 5). This supports the creation of the S_2 arcuate structure by a catastrophic flank collapse, which generated a large debris-avalanche deposit (Fig. 5). Despite careful inland search in the deepest valleys, we could not observe the volcanic sequence cut by S_2, because the scar has been covered by more recent cascading lava flows. In the western portion of S_2, especially, cascading lava flows partly formed a sub-aerial platform that is currently cut by S_3. We dated the base of S_3 as 69 ± 4 ka, and the base of the coastal cliff farther E as 43 ± 8 ka (Fig. 7A). From these new data, the catastrophic sector collapse here proposed occurred prior to ca. 69 ka. The maximum age of the collapse is more difficult to establish, especially as the possible connection

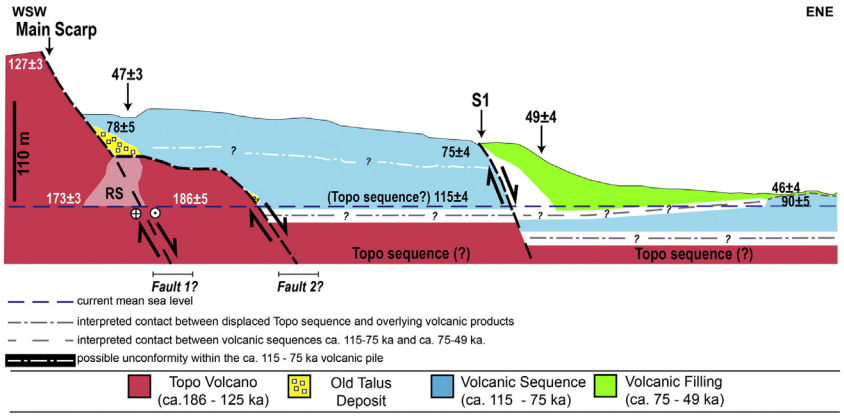

Fig. 8. Interpretative scheme of the slump structure.

between S_1 and S_2 remains enigmatic. As S_2 affects a domain previously occupied by Topo Volcano, we establish ca. 125 ka as the maximum age for S_2 formation. The sub-aerial part of S_2 truncates the previous lava succession(s) up to a height of ca. 600 m. From the volcanic pile(s) exposed immediately to the W of S_1, it seems plausible that the collapse removed not only the whole SE flank of the old volcanic edifice, but also part of the filling succession here dated between 115 ka and 75 ka (Fig. 7A). In such hypothesis, the catastrophic flank collapse here proposed possibly occurred between 75 ka and 69 ka. This narrow time interval coincides with the development of widespread volcanism along the whole Fissural System, as massive lava flows concealing the scars in the northern sector of the island yield similar ages (Fig. 3A, Costa et al., 2014). Parasitic scoria cones also developed close to the main scarp, upon the eroded remnants of the Topo Volcano, ca. 60 ka ago (Fig. 7A). Such apparent synchronicity supports a close link between volcanism and deformation along the various structures affecting the central part of the island. More recently, volcanic cones grew on S_2 (Fig. 7A), which coupled with the current distribution of subsidence in the slump area suggest that S_2 has accommodated gradual subsidence recently (Hildenbrand et al., 2012b). Similarly, the steepness of the exposed Main Scarp suggests that it accommodated movement recently.

Finally, S_3 constitutes a steep curvilinear scarp (Fig. 7A), whose orientation is compatible with the general orientation of the slump structures previously described. This scar cuts lava flows here dated at 69 ± 4 ka, and is partially blanketed in the west by volcanic deposits that form the lava delta here dated at 10 ± 2 ka (Fig. 7A). From the bathymetric data, it appears quite clear that this portion of the island flank partly sits on the submarine embayment associated with S_2, and therefore that it may be quite unstable. Therefore, we cannot exclude that the arcuate scarp S_3 formed by repeated detachment of coastal segments, prior to ca. 10 ka.

It is acknowledged that the evolution of a slump structure can lead to catastrophic destabilization (e.g., Moore et al., 1989, 1994; Urgeles et al., 1999). From the step-by-step evolution here presented, we conclude that Pico's SE flank slump evolved mostly through gradual deformation during the last 125 kyr, with the occurrence of a catastrophic flank collapse along S_2, most probably between ca. 75 and 69 ka. The consecutive local development of faults most probably potentiated the current focus of subsidence (Keating and McGuire, 2000; Hildenbrand et al., 2012b).

4.2. Comparison with other slumps and implications for flank movements on oceanic islands

The dimensions and subsidence rates of the studied slump are much smaller than those reported for the active Hilina slump(Kilauea's S flank) in Hawaii. Indeed, the Hilina Slump stretches at the surface ca. 50 km, which corresponds to the entire length of Pico Island. The subsidence rates in the Pico Slump are one order of magnitude smaller than those recorded for Hilina: up to 12 mm/yr during the 2006–2009 period for Pico's slump (Hildenbrand et al., 2012b), and up to 8 cm/yr during the 1990–1996 period for the Hilina Slump (Owen et al., 2000). The time constraint for the initiation of slumping in Hilina has been proposed to lie between 90–60 kyr (Smith et al., 1999). However, the geological record of the activity along Hilina's structures indicates 43 kyr (Riley et al., 1999; Okubo, 2004). The geological record and the new dating indicate that Pico's slump is older than Hilina, tracing the initiation of slumping in Pico back to, at least, ca. 115 ka. Many factors favouring/enabling large-scale flank movements on volcanic islands have been proposed (e.g., Keating and McGuire, 2000). A link between the occurrence of large-scale gravitational collapse in volcanic islands and climatic changes has been es pecially proposed (Carracedo et al., 1999), namely the coincidence of some of these events with transitions from glacial to interglacial periods (Quidelleur et al., 2008). Quidelleur et al. (2008) mentioned two occurrences for the glacial-interglacial transition comprised between ca. 140 and 125 ka: El Golfo 1 in El Hierro, Canaries (134 ± 6 ka, Carracedo et al., 1999), and Alika 2 in Hawaii (127 ± 5 ka, McMurthy et al., 1999). Germa et al. (2011) also reported the occurrence of a flank collapse at 127 ± 2 ka in Martinique Island (Lesser Antilles). This transitional period also overlaps with the age here determined for the initiation of Pico Slump: ca. 125–115 ka. On the other hand, the age constraints of the catastrophic events on the N and S flanks of Pico Island (ca. 125–70 ka, most probably ca. 75–69 ka for the collapse on the S flank), and propagation of the secondary slump structure S_1 correspond to a rather gradual/irregular transition from an interglacial to a glacial stage. This suggests that factors other than paleoclimatic changes controlled the occurrence of catastrophic collapse and slump development on Pico.

Unlike islands from archipelagos like Hawaii and Canaries, Pico Island has developed in a tectonically active area. The tectonic setting favoured its growth as a steep ridge, and, as shown in Fig. 1, its growth on top of a master normal fault making up the diffuse boundary between the Nubia and Eurasia plates. Therefore, we infer that the tectonic setting may have contributed significantly to the triggering of the catastrophic collapses here described for Pico, e.g. seismic activity and stress conditions favourable for dyke injection. For instance, we note that the composite collapse structure in SE Pico sits on the intersection of two main trends: (1) the WSW-ENE trend, which corresponds to the sharply cut sea cliff here interpreted as the result of a major fault, and to some of the dykes observed in the field (Fig. 3B). This trend corresponds to the local orientation expected for the transform faults of the Nubia-Eurasia plate boundary (DeMets et al., 2010; Marques et al., 2014b). (2) The WNW-ESE to E-W trend, which locally corresponds to the alignment of the headwall of the slump with the axis of the Fissural System, and regionally corresponds to the orientation of the main normal faults making up the diffuse Nu/Eu plate boundary.We note that earlier flank collapses recently recognized in Graciosa (Central Azores) and in S.

Miguel Island have also occurred along such directions (e.g., Sibrant et al., 2014, 2015b), reinforcing the role of regional tectonics as a major factor influencing/controlling flank movements in the Azores. Our study on Pico extends the record of past flank collapses in the Azores up to very recent times. As both regional tectonics setting and flank movements in Pico slump are still active, further catastrophic flank movements cannot be excluded, reinforcing the need to better monitor and study recent and present movements on the Faial-Pico ridge in the near future.

5. Conclusions

From the data/interpretations here presented, coupled with the results/interpretations presented in Costa et al. (2014), we propose the following long-term evolution of the slump in SE Pico Island:

1. The sub-aerial development of Topo Volcano lasted between ca. 186 and 125 ka, and possibly up to ca. 115 ka.
2. The destruction of Topo Volcano's N flank occurred between ca. 125 and 70 ka, with gradual subsidence along the Topo Fault and catastrophic deformation further N (probably already affecting deposits from the Fissural System, with associated generation of the submarine debris deposit reported in Costa et al., 2014). The gradual destruction of Topo's SE flank started between ca. 125 and 115 ka, generating the Main Scarp of the currently active slump (Hildenbrand et al., 2012b).
3. Between ca. 125 and 69 ka, the sub-aerial Fissural System grew substantially. In the same period, eastern Pico suffered catastrophic flank collapses: (1) on the N flank, with the occurrence of collapses directed towards the N, prior to ca. 69 ka on the westernmost scar, andbetween ca. 125 and 70 ka on the easternmost scar (event mentioned above, which destroyed the N flank of Topo Volcano); (2) on the S flank, along eastern S_2 (affecting the most distal sector of the subsided SE flank of Topo volcano) and generating the large debris deposit on the offshore, between ca. 125 and 69 ka (possibly between ca. 75 and 69 ka). This catastrophic collapse did not remove the whole of the unstable material, leaving behind a considerable volume of creeping rocks comprising the currently active Pico's slump.
4. Since ca. 70 ka, volcanic products erupted from the Fissural System, blanketing in great part the collapse scars. Around ca. 60 ka, parasitic cones developed unconformably on the SW flank of the Topo Volcano.
5. A slump is currently active in SE Pico (Hildenbrand et al., 2012b, 2013), possibly re-activating in-depth older mass-wasting structures.
6. The occurrence of catastrophic and gradual gravitational destabilization in Pico Island was conditioned by the active tectonic setting (interplate diffuse extensional deformation).

Further investigation should require additional onland and offshore data acquisition (e.g., seismic profiles) in order to constrain the in-depth geometry of the scars/slump structures, and the detailed configuration/volume of the inferred debris deposits.

Further modelling of flank instabilities should also be initiated to better constrain the controlling mechanisms and the susceptibility of the volcanic flanks to further gravitational collapse events.

Acknowledgments

This is a contribution to Project MEGAHazards (PTDC/CTE-GIX/108149/2008), funded by FCT, Portugal. ACGC had a PhD scholarship funded by FCT (SFRH/BD/68983/2010). ACGC wishes to acknowledge Judite Costa, José Costa and José Dias for the support in the fieldwork. We acknowledge EMEPC (Estrutura de Missão para a Extensão da Plataforma Continental) for providing the high-resolution bathymetric data used here. The final version of this paper benefited from the constructive and thorough comments by the reviewer R. Quartau, and editor J. Marti.

Appendix A. Supplementary data

Supplementary data to this article can be found online at http://dx.doi.org/10.1016/j.jvolgeores.2015.06.008.

References

Borges, J.F., Bezzeghoud, M., Buforn, E., Pro, C., Fitas, A., 2007. The 1980, 1997 and 1998 Azores earthquakes and some seismo-tectonic implications. Tectonophysics 435 (1—4), 37–54. http://dx.doi.org/10.1016/j.tecto.2007.01.008.

Boudon, G., Le Friant, A., Komorowski, J.-C., Deplus, C., Semet, M.P., 2007. Volcano flank instability in the Lesser Antilles Arc: Diversity of scale, processes, and temporal recurrence. J. Geophys. Res. 112, B08205. http://dx.doi.org/10.1029/2006JB004674.

Boulesteix, T., Hildenbrand, A., Gillot, P.Y., Soler, V., 2012. Eruptive response of oceanic islands to giant landslides: new insights from the geomorphologic evolution of the Teide–Pico Viejo volcanic complex (Tenerife, Canary). Geomorphology 138 (1), 61–73. http://dx.doi.org/10.1016/j.geomorph.2011.08.025.

Boulesteix, T., Hildenbrand, A., Soler, V., Quidelleur, X., Gillot, P.Y., 2013. Coeval giant landslides in the Canary Islands: implications for global, regional and local triggers of giant flank collapses on oceanic volcanoes. J. Volcanol. Geotherm. Res. 257, 90–98. http://dx.doi.org/10.1016/j.jvolgeores.2013.03.008.

Carracedo, J.C., 1994. The Canary Islands: an example of structural control on the growth of large oceanic-island volcanoes. J. Volcanol. Geotherm. Res. 60, 225–241.

Carracedo, J.C., Day, S.J., Guillou, H., Torrado, F.J.P., 1999. Giant Quaternary landslides in the evolution of La Palma and El Hierro, Canary Islands. J. Volcanol. Geotherm. Res. 94, 169–190. http://dx.doi.org/10.1016/S0377-0273(99)00102-X.

Cassignol, C., Gillot, P.Y., 1982. Range and effectiveness of unspiked potassium–argon dating: experimental groundwork and applications. In: Odin, G.S. (Ed.), Numerical dating in stratigraphy. John Wiley & Sons Ltd, Chichester, England, pp. 159–179.

Chovelon, P., 1982. Evolution volcanotectonique des iles de Faial et de Pico Ph.D. Thesis, Univ. Paris-Sud, Orsay, France (186 pp.).

Clouard, V., Bonneville, A., 2004. Submarine Landslides in French Polynesia. In: Hekinian, R., Stoffers, P., Cheminé, J.-L. (Eds.), Oceanic Hotspots: intraplate submarine magmatism and tectonism. Springer-Verlag, pp. 209–238.

Clouard, V., Bonneville, A., Gillot, P.Y., 2001. A giant landslide on the southern flank of Tahiti Island, French Polynesia. Geophys. Res. Lett. 28, 2253–2256.

Costa, A.C.G., Marques, F.O., Hildenbrand, A., Sibrant, A.L.R., Catita, C.M.S., 2014. Large-scale catastrophic flank collapses in a steep volcanic ridge: The Pico–Faial Ridge, Azores Triple Junction. J. Volcanol. Geotherm. Res. 272, 111–125. http://dx.doi.org/10.1016/j.jvolgeores.2014.01.002.

Day, S.J., Heleno da Silva, S.I.N., Fonseca, J.F.B.D., 1999. A past giant lateral collapse and present-day flank instability of Fogo, Cape Verde Islands. J. Volcanol. Geotherm. Res. 94 (1–4), 191–218. http://dx.doi.org/10.1016/S0377-0273(99)00103-1.

Demande, J., Fabriol, R., Gérard, A., Iundt, F., 1982. Prospection géothermique des Iles de Faial et Pico (Açores). Report 82SGN003GTH. Bureau de Recherches Géologiques et Minières, Orléans, France.

DeMets, C., Gordon, R.G., Argus, D.F., 2010. Geologically current plate motions. Geophys. J. Int. 181, 1–80. http://dx.doi.org/10.1111/j.1365-246X.2009.04491.x.

Féraud, G., Kaneoka, I., Allègre, C.J., 1980. K/Ar ages and stress pattern in the Azores: geodynamic implications. Earth Planet. Sci. Lett. 46 (2), 275–286. http://dx.doi.org/10.1016/0012-821X(80)90013-8.

Fernandes, R.M.S., Bastos, L., Miranda, J.M., Lourenço, N., Ambrosius, B.A.C., Noomen, R., Simons, W., 2006. Defining the plate boundaries in the Azores region. J. Volcanol. Geotherm. Res. 156 (1–2), 1–9. http://dx.doi.org/10.1016/j.jvolgeores.2006.03.019.

Forjaz, V.H., 1966. Carta geológica do sistema vulcânico Faial-Pico-S. Jorge. Escala 1:200 000. In: Machado, F., Forjaz, V.H., (Eds.), A actividade vulcânica na ilha do Faial (1957-67), 1968, Comissão de Turismo da Horta, Portugal, 89 pp.

Forjaz, V.H., Serralheiro, A., Nunes, J.C., 1990. Carta vulcanológica dos Açores - Grupo Central. Escala 1:200000. Serviço Regional de Protecção Civil, Universidade dos Açores e Centro de Vulcanologia INIC, Ponta Delgada, Portugal.

França, Z., 2000. Origem e evolução petrológica e geoquímica do vulcanismo da ilha do Pico. Açores Ph.D. Thesis. Univ. Açores, Ponta Delgada, Portugal.

França, Z., Nunes, J.C., Cruz, J.V., Carvalho, M.R., Serralheiro, A., 2000. Carta de distribuição petrográfica da ilha do Pico (Açores) e mapa de amostragem. In: França, Z. (Ed.), Origem e evolução petrológica e geoquímica do vulcanismo da ilha do Pico - Açores, 2002. Câmara Municipal de São Roque do Pico, Portugal (391 pp.).

França, Z.T.M., Tassinari, C.C.G., Cruz, J.V., Aparicio, A.Y., Araña, V., Rodrigues, N.R., 2006. Petrology, geochemistry and Sr-Nd-Pb isotopes of the volcanic rocks from Pico Island - Azores (Portugal). J. Volcanol. Geotherm. Res. 156 (1–2), 71–89. http://dx.doi.org/10.1016/j.jvolgeores.2006.03.013.

Germa, A., Quidelleur, X., Lahitte, P., Labanieh, S., Chauvel, C., 2011. The K–Ar Cassignol Gillot technique applied to western Martinique lavas: a record of Lesser Antilles arc activity from 2 Ma to Mount Pelée volcanism. Quat. Geochronol. 6 (3–4), 341–355. http://dx.doi.org/10.1016/j.quageo.2011.02.001.

Gillot, P.Y., Cornette, Y., 1986. The Cassignol technique for potassium–argon dating, precision and accuracy: examples from the Late Pleistocene to Recent volcanics from southern Italy. Chem. Geol. Isot. Geosci. Sect. 59, 205–222. http://dx.doi.org/10.1016/0168-9622(86)90072-2.

Gillot, P.Y., Hildenbrand, A., Lefèvre, J.C., Albore-Livadie, C., 2006. The K/Ar dating method: principle, analytical techniques and application to Holocene volcanic eruptions in Southern Italy. Acta Vulcanol. 18, 55–66.
Hildenbrand, A., Gillot, P.Y., Le Roy, I., 2004. Volcano-tectonic and geochemical evolution of an oceanic intra-plate volcano: Tahiti-Nui (French Polynesia). Earth Planet. Sci. Lett. 217 (3–4), 349–365. http://dx.doi.org/10.1016/S0012-821X(03)00599-5.
Hildenbrand, A., Gillot, P.Y., Bonneville, A., 2006. Offshore evidence for a huge landslide of the northern flank of Tahiti–Nui (French Polynesia). Geochem. Geophys. Geosyst. 7 (3), Q03006. http://dx.doi.org/10.1029/2005GC001003.
Hildenbrand, A., Madureira, P., Ornelas Marques, F., Cruz, I., Henry, B., Silva, P., 2008. Multi-stage evolution of a sub-aerial volcanic ridge over the last 1.3 Myr: S. Jorge Island, Azores Triple Junction. Earth Planet. Sci. Lett. 273 (3–4), 289–298. http://dx.doi.org/10.1016/j.epsl.2008.06.041.
Hildenbrand, A., Marques, F.O., Costa, A.C.G., Sibrant, A.L.R., Silva, P.M.F., Henry, B., Miranda, J.M., Madureira, P., 2012a. Reconstructing the architectural evolution of volcanic islands from combined K/Ar, morphologic, tectonic, and magnetic data: the Faial Island example (Azores). J. Volcanol. Geotherm. Res. 241–242, 39–48. http://dx.doi.org/10.1016/j.jvolgeores.2012.06.019.
Hildenbrand, A., Marques, F.O., Catalão, J., Catita, C.M.S., Costa, A.C.G., 2012b. Large-scale active slump of the southeastern flank of Pico Island, Azores. Geology 40 (10), 939–942. http://dx.doi.org/10.1130/G33303.1.
Hildenbrand, A., Marques, F.O., Catalão, J., Catita, C.M.S., Costa, A.C.G., 2013. Large-scale active slump of the southeastern flank of Pico Island, Azores: reply. Geology 41 (12), e302. http://dx.doi.org/10.1130/G34879Y.1.
Hildenbrand, A., Weis, D., Madureira, P., Marques, F.O., 2014. Recent plate re-organization at the Azores Triple Junction: Evidence from combined geochemical and geochronological data on Faial, S. Jorge and Terceira volcanic islands. Lithos 210–211, 27–39. http://dx.doi.org/10.1016/j.lithos.2014.09.009.
Hipólito, A., Madeira, J., Carmo, R., Gaspar, J.L., 2013. Neotectonics of Graciosa island (Azores): a contribution to seismic hazard assessment of a volcanic area in a complex geodynamic setting. Ann. Geophys. 56 (6), S0677. http://dx.doi.org/10.4401/ag-6222.
Keating, B.H., McGuire, W.J., 2000. Island edifice failures and associated tsunami hazards. Pure Appl. Geophys. 157 (6–8), 899–955.
Krastel, S., Schmincke, H.U., Jacobs, C.L., Rihm, R., Le Bas, T.P., Alibés, B., 2001. Submarine landslides around the Canary Islands. J. Geophys. Res. 106 (B3), 3977–3997. http://dx.doi.org/10.1029/2000JB900413.
Lipman, P.W., Normark, W.R., Moore, J.G., Wilson, J.B., Gutmacher, C.E., 1988. The giant submarine Alika debris slide, Mauna Loa, Hawaii. J. Geophys. Res. Solid Earth 93 (B5), 4279–4299. http://dx.doi.org/10.1029/JB093iB05p04279.
Lourenço, N., 2007. Tectono-magmatic Processes at the Azores Triple Junction Ph.D. Thesis, Univ. Algarve, Faro, Portugal (239 pp.).
Lourenço, N., Miranda, J.M., Luis, J.F., Ribeiro, A., Mendes Victor, L.A., Madeira, J., Needham, H.D., 1998. Morpho-tectonic analysis of the Azores Volcanic Plateau from a new bathymetric compilation of the area. Mar. Geophys. Res. 20 (3), 141–156. http://dx.doi.org/10.1023/A%3A1004505401547.
Luis, J.F., Miranda, J.M., 2008. Reevaluation of magnetic chrons in the North Atlantic between 35°N and 47°N:Implications for the formation of the Azores Triple Junction and associated plateau. J. Geophys. Res. 113 (B10), B10105. http://dx.doi.org/10.1029/2007JB005573.
Luis, J.F., Miranda, J.M., Galdeano, A., Patriat, P., 1998. Constraints on the structure of the Azores spreading center from gravity data. Mar. Geophys. Res. 20 (3), 157–170. http://dx.doi.org/10.1023/A:1004698526004.
Machado, F., Trêpa, M.V., Férin, C., Nunes, J.C., 1974. Crise sísmica do Pico (Açores), Nov. 1973. Comunicações dos Serviços Geológicos de Portugal 57 pp. 229–242.
Madeira, J., 1998. Estudos de neotectónica nas ilhas do Faial, Pico e S. Jorge: Uma contribuição para o conhecimento geodinâmico da junção tripla dos Açores Ph.D. Thesis, Univ. Lisboa, Portugal (481 pp.).
Madeira, J., Brum da Silveira, A., 2003. Active tectonics and first paleoseismological results in Faial, Pico and S. Jorge islands (Azores, Portugal). Ann. Geophys. 46 (5), 733–761. http://dx.doi.org/10.4401/ag-3453.
Manconi, A., Longpre, M.A., Walter, T.R., Troll, V.R., Hansteen, T.H., 2009. The effects of flank collapses on volcano plumbing systems. Geology 37 (12), 1099–1102. http://dx.doi.org/10.1130/G30104A.1.
Marques, F.O., Catalão, J.C., DeMets, C., Costa, A.C.G., Hildenbrand, A., 2013a. GPS and tectonic evidence for a diffuse plate boundary at the Azores Triple Junction. Earth Planet. Sci. Lett. 381, 177–187. http://dx.doi.org/10.1016/j.epsl.2013.08.051.
Marques, F.O., Sibrant, A.L.R., Hildenbrand, A., Costa, A.C.G., 2013b. Large-scale sector collapses in the evolution of Santa Maria Island, Azores. Abstract Meeting AGU, 2013.
Marques, F.O., Catalão, J.C., DeMets, C., Costa, A.C.G., Hildenbrand, A., 2014a. Corrigendum to "GPS and tectonic evidence for a diffuse plate boundary at the Azores Triple Junction" [Earth Planet. Sci. Lett. 381 (2013) 177–187]. Earth Planet. Sci. Lett. 387, 1–3. http://dx.doi.org/10.1016/j.epsl.2013.11.029.
Marques, F.O., Catalão, J., Hildenbrand, A., Costa, A.C.G., Dias, N.A., 2014b. The 1998 Faial earthquake, Azores: Evidence for a transform fault associated with the Nubia-Eurasia plate boundary? Tectonophysics http://dx.doi.org/10.1016/j.tecto.2014.06.024.
Masson, D.G., Watts, A.B., Gee, M.J.R., Urgeles, R., Mitchell, N.C., Le Bas, T.P., Canals, M., 2002. Slope failures on the flanks of the western Canary Islands. Earth Sci. Rev. 57 (1–2), 1–35. http://dx.doi.org/10.1016/S0012-8252(01)00069-1.
Masson, D.G., Le Bas, T.P., Grevemeyer, I., Weinrebe, W., 2008. Flank collapse and largescale landsliding in the Cape Verde Islands, off West Africa. Geochem. Geophys. Geosyst. 9 (7), Q07015. http://dx.doi.org/10.1029/2008GC001983.
McMurthy, G.M., Herrero-Bervera, E., Cremer, M.D., Smith, J.R., Resig, J., Sherman, C., Torresan, M.E., 1999. Stratigraphic constraints on the timing and emplacement of the Alika 2 giant submarine landslide. J. Volcanol. Geotherm. Res. 94 (1-4), 35–58. http://dx.doi.org/10.1016/S0377-0273(99)00097-9.
Miranda, J.M., Mendes Victor, L.A., Simões, J.Z., Luis, J.F., Matias, L., Shimamura, H., Shiobara, H., Nemoto, H., Mochizuki, H., Hirn, A., Lépine, J.C., 1998. Tectonic setting of the Azores Plateau deduced from a OBS survey. Mar. Geophys. Res. 20, 171–182.
Miranda, J.M., Luis, J.F., Lourenço, N., Goslin, J., 2014. Distributed deformation close to the Azores Triple "Point". Mar. Geol. 355, 27–35. http://dx.doi.org/10.1016/j.margeo.2014.05.006.
Mitchell, N.C., 2003. Susceptibility of mid-ocean ridge volcanic islands and seamounts to large-scale landslding. J. Geophys. Res. 108 (B8), 2397. http://dx.doi.org/10.1029/2002JB001997.
Mitchell, N.C., Beier, C., Rosin, P.L., Quartau, R., Tempera, F., 2008. Lava penetrating water: submarine lava flows around the coasts of Pico Island, Azores. Geochem. Geophys. Geosyst. 9 (3), Q03024. http://dx.doi.org/10.1029/2007GC001725.
Mitchell, N.C., Quartau, R., Madeira, J., 2012a. Assessing landslide movements in volcanic islands using near-shore marine geophysical data: south Pico Island, Azores. Bull. Volcanol. 74 (2), 483–496. http://dx.doi.org/10.1007/s00445-011-0541-5.
Mitchell, N.C., Stretch, R., Oppenheimer, C., Kay, D., Beier, C., 2012b. Cone morphologies associated with shallow marine eruptions: east Pico Island, Azores. Bull. Volcanol. 74 (10), 2289–2301. http://dx.doi.org/10.1007/s00445-012-0662-5.
Mitchell, N.C., Quartau, R., Madeira, J., 2013. Large-scale active slump of the southeastern flank of Pico Island, Azores: comment. Geology 41 (12), e301. http://dx.doi.org/10.1130/G34006C.1.
Moore, J.G., Clague, D.A., 2002. Mapping the Nuuanu andWailau Landslides in Hawaii. In: Takahashi, E., Lipman, P.W., Garcia, M.O., Naka, J., Aramaki, S. (Eds.), Hawaiian volcanoes: deep underwater perspectivesGeophysical Monograph Series 128. American Geophysical Union, Washington D.C., pp. 223–244. http://dx.doi.org/10.1029/GM128.
Moore, J.G., Clague, D.A., Holcomb, R.T., Lipman, P.W., Normark, W.R., Torresan, M.E., 1989. Prodigious submarine landslides on the Hawaiian Ridge. J. Geophys. Res. 94 (B12), 17465–17484. http://dx.doi.org/10.1029/JB094iB12p17465.
Moore, J.G., Normark, W.R., Holcomb, R.T., 1994. Giant Hawaiian landslides. Annu. Rev. Earth Planet. Sci. 22, 119–144. http://dx.doi.org/10.1146/annurev.ea.22.050194.001003.
Neves, M.C., Miranda, J.M., Luis, J.F., 2013. The role of lithospheric processes on the development of linear volcanic ridges in the Azores. Tectonophysics 608, 376–388. http://dx.doi.org/10.1016/j.tecto.2013.09.016.
Normark, W.R., Moore, J.G., Torresan, M.E., 1993. Giant Volcano-Related Landslides and the Development of the Hawaiian Islands. In: Schwab, W.C., Lee, H.J., Twichell, D.C. (Eds.), Submarine landslides: Selected studies in the U.S. Exclusive Economic Zone, 2002. U.S. Geological Survey Bulletin, pp. 184–196.
Nunes, J.C., 1999. A actividade vulcânica na ilha do Pico do Plistocénico Superior ao Holocénico: Mecanismo eruptivo e hazard vulcânico Ph.D. Thesis, Univ. Açores, Ponta Delgada, Portugal (356 pp., available at: http://www.jcnunes.uac.pt/principal.htm).
Nunes, J.C., 2002. Lateral collapse structures in Pico Island (Azores): mechanism, constraints and age. 3a Assembleia Luso Espanhola de Geodesia e Geofísica, Valencia, pp. 731–735.
Nunes, J.C., França, Z., Cruz, J.V., Carvalho, M.R., Serralheiro, A., 1999a. Carta Vulcanológica da Ilha do Pico (Açores). In: Nunes, J.C. (Ed.), A actividade vulcânica na ilha do Pico do Plistocénico Superior ao Holocénico: Mecanismo eruptivo e hazard vulcânico, 1999. Univ. Açores, Ponta Delgada, Portugal (Ph.D. Thesis, 356 pp.).
Nunes, J.C., França, Z., Cruz, J.V., Carvalho, M.R., Serralheiro, A., 1999b. Carta Morfotectónica da Ilha do Pico (Açores). In: Nunes, J.C. (Ed.), A actividade vulcânica na ilha do Pico do Plistocénico Superior ao Holocénico: Mecanismo eruptivo e hazard vulcânico, 1999. Univ. Açores, Ponta Delgada, Portugal (Ph.D. Thesis, 356 pp.).
Nunes, J.C., Camacho, A., França, Z., Montesinos, F.G., Alves, M., Vieira, R., Velez, E., Ortiz, E., 2006. Gravity anomalies and crustal signature of volcano-tectonic structures of Pico Island (Azores). J. Volcanol. Geotherm. Res. 156 (1–2), 55–70. http://dx.doi.org/10.1016/j.jvolgeores.2006.03.023.
Okubo, C.H., 2004. Rock mass strength and slope stability of the Hilina slump, Kilauea volcano, Hawai'i. J. Volcanol. Geotherm. Res. 138, 43–76. http://dx.doi.org/10.1016/j.jvolgeores.2004.06.006.
Owen, S., Segall, P., Lisowski, M., Miklius, A., Denlinger, R., Sako, M., 2000. Rapid deformation of Kilauea Volcano: Global Positioning System measurements between 1990 and 1996. J. Geophys. Res. 105 (B8), 2156–2202. http://dx.doi.org/10.1029/2000JB900109.
Quidelleur, X., Hildenbrand, A., Samper, A., 2008. Causal link between Quaternary paleoclimatic changes and volcanic islands evolution. Geophys. Res. Lett. 35, L02303. http://dx.doi.org/10.1029/2007GL031849.
Ramalho, R.S., Quartau, R., Trenhaile, A.S., Mitchell, N.C., Woodroffe, C.D., Ávila, S.P., 2013. Coastal evolution on volcanic islands: A complex interplay between volcanism, erosion, sedimentation, sea-level change and biogenic production. Earth Sci. Rev. 127, 140–170. http://dx.doi.org/10.1016/j.earscirev.2013.10.007.
Ricci, J., Lahitte, P., Quidelleur, X., 2015. Construction and destruction rates of volcanoes within tropical environment: Examples from the Basse-Terre Island (Guadeloupe, Lesser Antilles). Geomorphology 228, 597–607. http://dx.doi.org/10.1016/j.geomorph.2014.10.002.
Riley, C.M., Diehl, J.F., Kirschvink, J.L., Ripperdan, R.L., 1999. Paleomagnetic constraints on fault motion in the Hilina Fault System, south flank of Kilauea Volcano, Hawaii. J. Volcanol. Geotherm. Res. 94 (1–4), 233–249. http://dx.doi.org/10.1016/S0377-0273(99)00105-5.
Samper, A., Quidelleur, X., Lahitte, P., Mollex, D., 2007. Timing of effusive volcanism and collapse events within an oceanic arc island: Basse–Terre, Guadeloupe archipelago (Lesser Antilles Arc). Earth Planet. Sci. Lett. 258 (1–2), 175–191. http://dx.doi.org/10.1016/j.epsl.2007.03.030.
Satake, K., Smith, J.R., Shinozaki, K., 2002. Three-dimensional reconstruction and tsunami model of the Nuuanu and Wailau giant landslides, Hawaii. In: Takahashi, E., Lipman, P.W., Garcia, M.O., Naka, J., Aramaki, S. (Eds.), Hawaiian volcanoes: Deep underwater

perspectivesGeophysical Monograph Series 128. American Geophysical Union, Washington D.C., pp. 333–346. http://dx.doi.org/10.1029/GM128.

Sibrant, A.L.R., Marques, F.O., Hildenbrand, A., 2014. Construction and destruction of a volcanic island developed inside an oceanic rift: Graciosa Island, Terceira Rift, Azores. J. Volcanol. Geotherm. Res. 284, 32–45. http://dx.doi.org/10.1016/j.jvolgeores.2014.07.014.

Sibrant, A.L.R., Hildenbrand, A., Marques, F.O., Costa, A.C.G., 2015a. Volcano-tectonic evolution of the Santa Maria Island (Azores): Implications for paleostress evolution at the western Eurasia-Nubia plate boundary. Volcanol. Geotherm. Res. 291, 49–62. http://dx.doi.org/10.1016/j.jvolgeores.2014.12.017.

Sibrant, A.L.R., Hildenbrand, A., Marques, F.O., Weiss, B., Boulesteix, T., Hübscher, C., Lüdmann, T., Costa, A.C.G., Catalão, J.C., 2015b. Morpho-structural evolution of a volcanic island developed inside an active oceanic rift: S. Miguel Island (Terceira Rift, Azores). Volcanol. Geotherm. Res. http://dx.doi.org/10.1016/j.jvolgeores.2015.04.011.

Smith, J.R., Malahoff, A., Shor, A.N., 1999. Submarine geology of the Hilina slump and morpho-structural evolution of Kilauea volcano, Hawaii. J. Volcanol. Geotherm. Res. 94, 59–88. http://dx.doi.org/10.1016/S0377-0273(99)00098-0.

Steiger, R.H., Jäger, E., 1977. Subcommission on geochronology: convention on the use of decay constants in geo- and cosmochronology. Earth Planet. Sci. Lett. 36 (3), 359–362. http://dx.doi.org/10.1016/0012-821X(77)90060-7.

Stretch, R., Mitchell, N.C., Portaro, R.A., 2006. A morphometric analysis of the submarine volcanic ridge of Pico Island. J. Volcanol. Geotherm. Res. 156 (1–2), 35–54. http://dx.doi.org/10.1016/j.jvolgeores.2006.03.009.

Trippanera, D., Porreca, M., Ruch, J., Pimentel, A., Acocella, V., Pacheco, J., Salvatore, M., 2013. Relationships between tectonics and magmatism in a transtensive/transform setting: An example from Faial Island (Azores, Portugal). Geol. Soc. Am. Bull. 126 (1–2), 164–181. http://dx.doi.org/10.1130/B30758.1.

Urgeles, R., Masson, D.G., Canals, M., Watts, A.B., Le Bas, T., 1999. Recurrent large-scale landsliding on the west flank of La Palma, Canary Islands. J. Geophys. Res. Solid Earth 104 (B11), 25331–25348. http://dx.doi.org/10.1029/1999JB900243.

Woodhall, D., 1974. Geology and volcanic history of Pico Island Volcano, Azores. Nature 248, 663–665. http://dx.doi.org/10.1038/248663a0.

Zbyszewski, G., Ribeiro Ferreira, C., Veiga Ferreira, O., Torre de Assunção, C., 1963. Notícia explicativa da Folha "B" da Ilha do Pico (Açores). Carta Geológica de Portugal na escala 1/50 000. Serviços Geológicos de Portugal. Lisbon, Portugal. 21 pp.

APPPENDIX A

DEM origin and construction

The sub-aerial topographic data here presented were produced from the digital topographic map of Pico Island (Portuguese Army Geographic Institute), of 1:25,000 scale and vertical accuracy of ca. 5 m (Afonso et al., 2002). Details on the sub-aerial DEM construction are provided in Costa et al. (2014). The DEMs presented for Pico and Faial islands have spatial resolution of 10 and 50 m, respectively.

The 50-250m resolution submarine data here presented resulted from a swath bathymetry survey with a 12 kHz Kongsberg EM120 multibeam echo sounder system. The estimated depth accuracy (RMS, Root Mean Square) is 0.2-0.5% of the water depth (Kongsberg, 2007). As the maximum depth of the presented high-resolution area is ca. 1750 m, the maximum RMS estimated for these data ranges between 3.5-8.75 m. The data were processed using CARIS software, clean of noise and converted to an ASCII file. Afterwards, these data were converted to a raster structure of either 50 m or 250 m spatial resolution, using kriging spatial interpolation. The grid displaying these submarine data (Figs. 4 and 5) was built from a composition of data from different sources and of different resolutions (Fig. 4a): (a) the sub-aerial data of 10 m resolution (green area in Fig.4a); (b) the submarine 50 and 250 m data (grey and light blue areas, respectively, in Fig. 4a); (c) 100 m spaced depth contours for the shallow depths adjacent to the scar on Pico's SE flank (Figs. 2b and 2c), obtained from photogrammetry of Fig. 1a in Mitchell et al. (2012) (black lines in Fig.4a); (d) 1000 m resolution bathymetric data (blue dots in Fig. 4a, Lourenço et al.,1998). First we performed a spatial interpolation of 200 m resolution on the submarine domain, considering the data distribution represented in Fig. 4a. The WSW-ESE apparent alignments visible on the shaded reliefs from Figs. 4b and 4c, are artefacts related to the spatial interpolation of the

contour levels (Fig. 4a). Afterwards, we composed the final 50 m resolution grid mosaic, considering preferentially the 50/250 m resolution bathymetric data and the 10 m resolution sub-aerial data, and filling the remaining space with the 200 m resolution data from the interpolation performed previously.

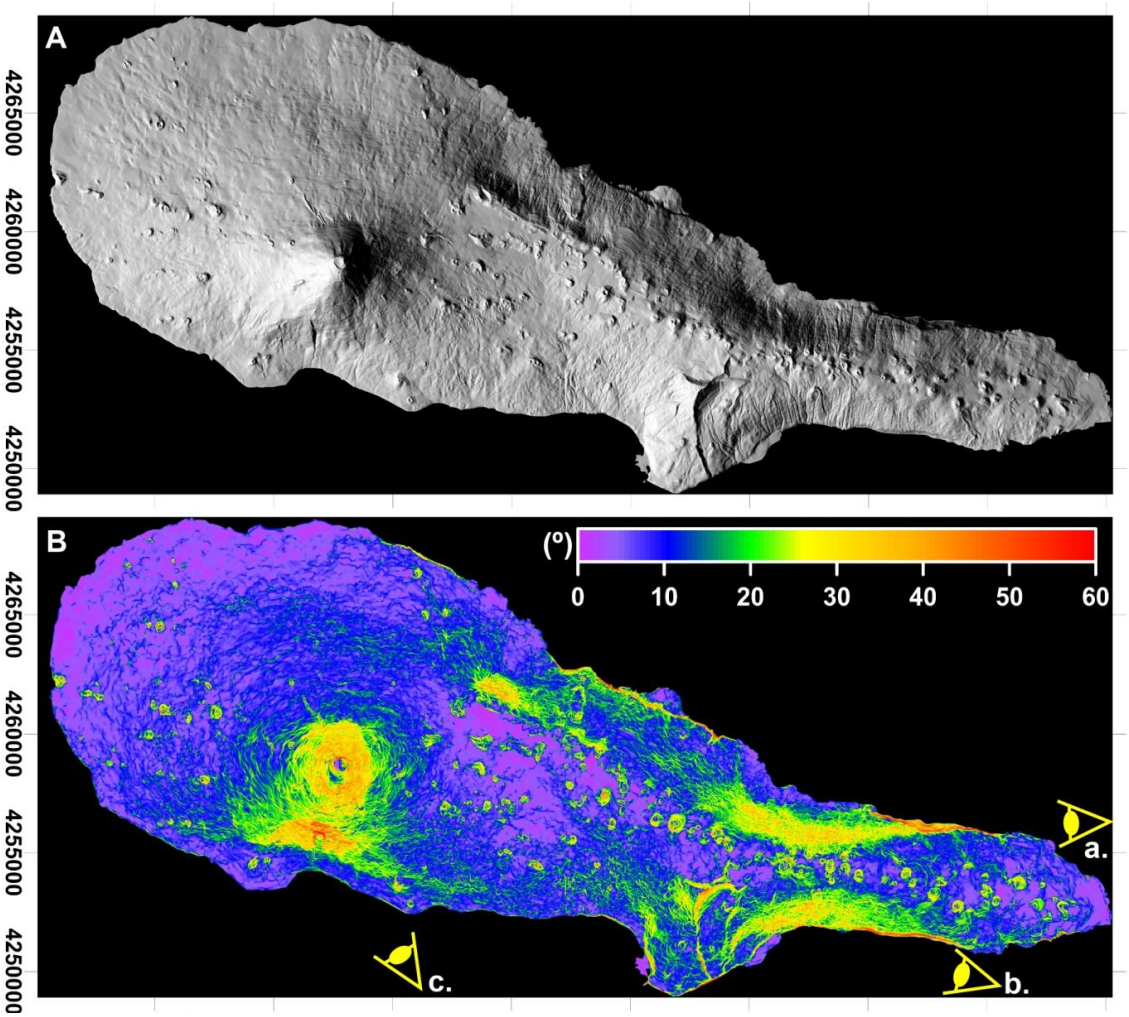

Fig. A.1. (A) Shaded relief of the 10 m resolution DEM of Pico Island (lighting from WSW), with coordinates in metres UTM (zone 26N). **(B)** Slope map of Pico Island built from the 10 m resolution DEM. 3D perspectives indicated as yellow eyes are presented in Fig. A.2. "a." - view presented in Fig. A.2a. Perspective "b." - view presented in Fig. A.2b. Perspective "c." - view presented in Fig. A.2c.

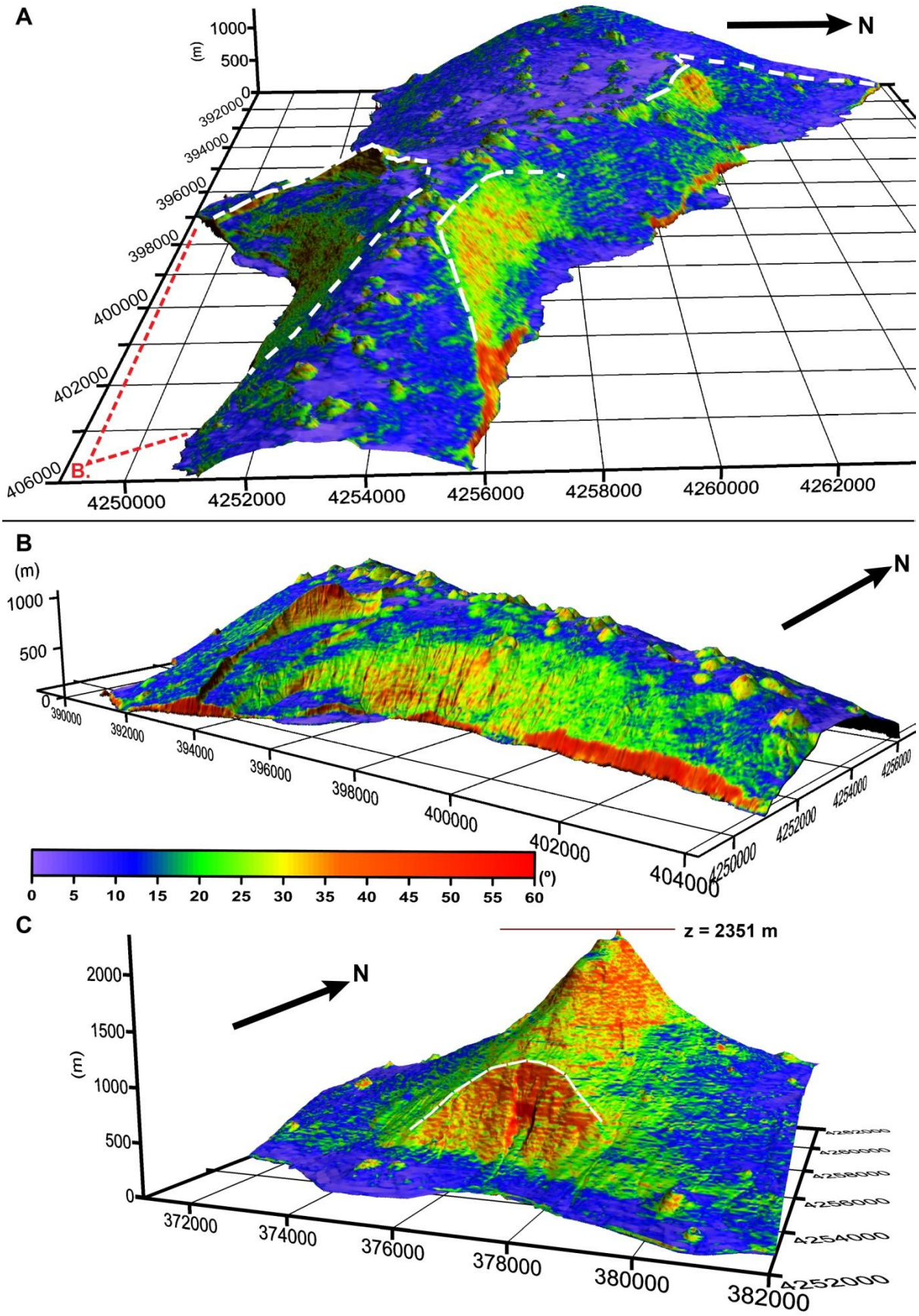

Fig. A.2. Images obtained by superimposing the 3D view of Pico Island relief (vertical

exaggeration: 2x) and the slope map image (shared color scale for slope angles), obtained from a 10 m resolution DEM. Perspectives presented A, B and C, are indicated in Fig. 2b by "i.", "C." and "ii.", respectively. **(A)** Perspective from E (lighting from NW), of Pico Island's topography, with interpretation of the N and S flanks' main scarps as dashed white lines. **(B)** View from ESE of the slump structure's topography (lighting from SW). The interpreted slump structures are presented in Fig. 2c. **(C)** Perspective from SE of Pico stratovolcano's strongly dipping southern flank (lighting from SE).

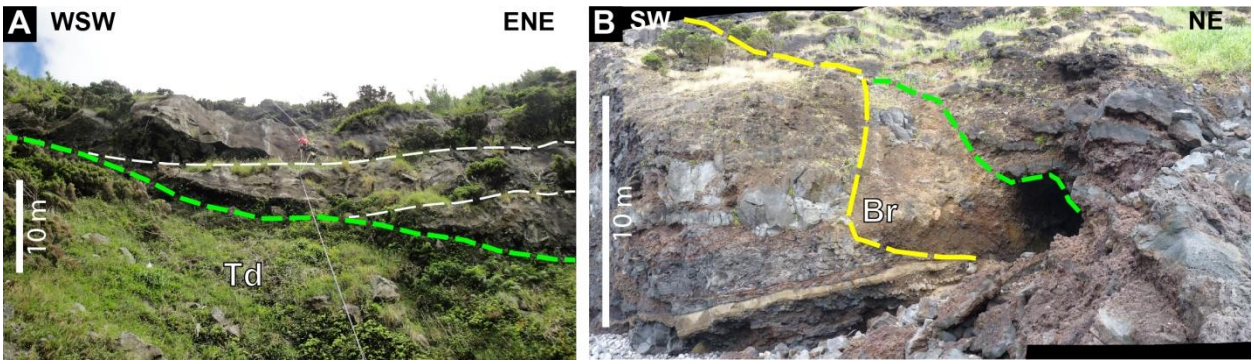

Figure A.3. (A) and (B) are zoomed pictures of the areas limited by the green rectangles *a* and *b* in Fig.3c, respectively. (A) Detail of the wedge-shaped talus deposit (Td), covered by lava flows (green dashed line - upper contour of the Td; white dashed lines - basal contour of the lava flows). (B) Breccia (Br) covering the eastern edge of the footwall block (yellow dashed line), and overlain by a lava flow sequence (green dashed line).

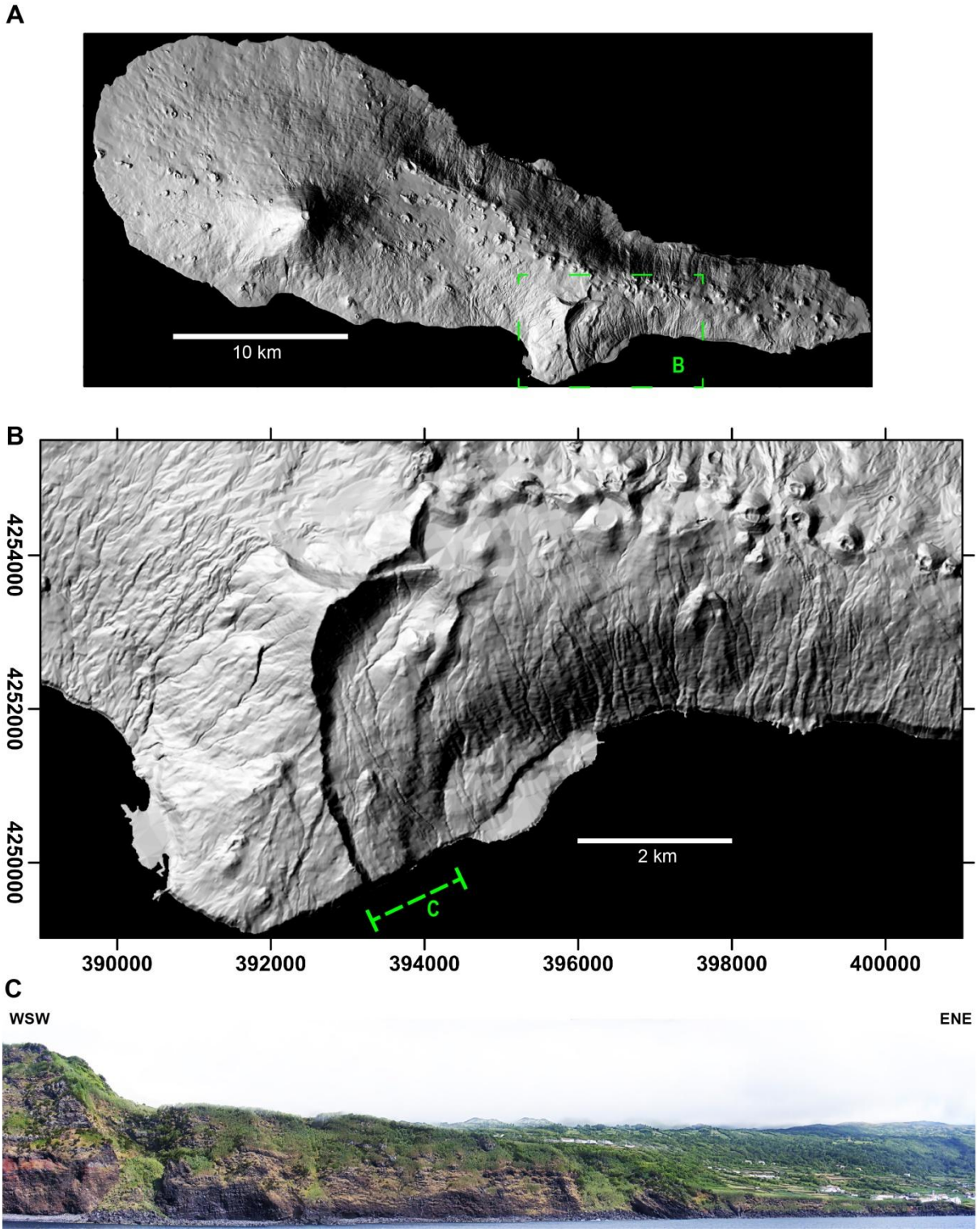

Fig. A.4. (A) Shaded relief of Pico Island from a 10 m resolution DEM (lighting from WSW). **(B)** Shaded relief of Pico Island from a 10 m resolution DEM (lighting from NW). **(C)** WSW-ENE view of the sea cliff whose extent is indicated as a green dashed line in (B).

Fig. A.5. Zoom in on the sea cliff presented as Fig. A.4c.

Fig. A.6. Interpretation of the sea cliff section presented in Figs. A.4c and A.5. Yellow

dashed line indicates possible unconformity. Full red line represents a main physical discontinuity. The samples collected on this sea cliff are indicated in **A**.

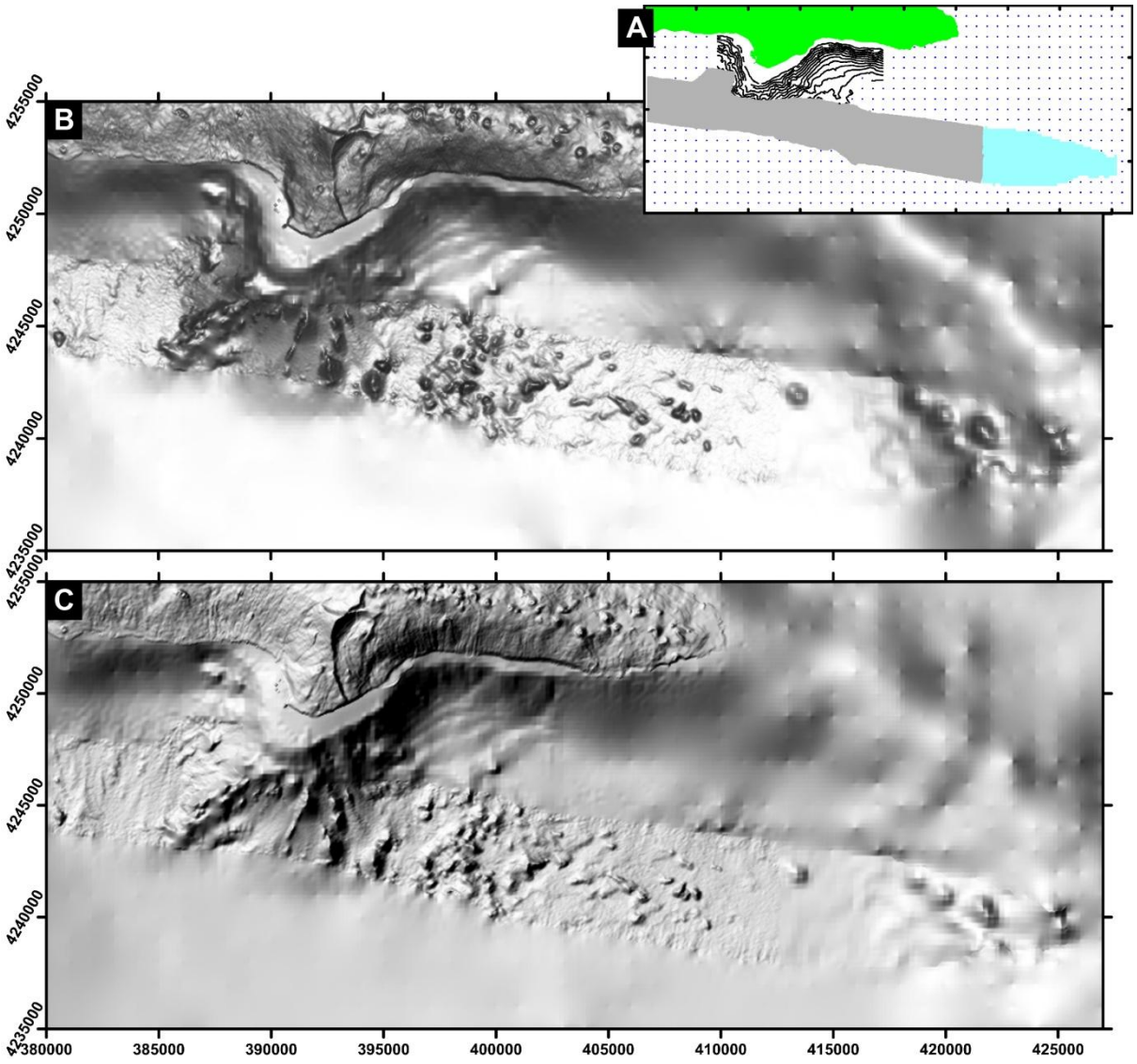

Fig. A.7. (A) Different elements used to composed the 50m resolution grid presented below: green - 10 m resolution sub-aerial DEM; blue - 250m resolution bathymetric data (made available by EMEPC); grey - 50m resolution bathymetric data (made available by EMEPC); black lines - depth contours from Fig. 1b in Mitchell et al. (2012); blue dots - bathymetric data extracted from the 1000 m resolution grid from Lourenço et al. (1998), available at http://w3.ualg.pt/~jluis/acores_plateau.htm. **(B)** and **(C)** constitute shaded reliefs from the 50m resolution grid composed as described in (A), with vertical lighting and lighting from

WNW, respectively. The apparent WSW-ENE lineaments visible in the area of interpolation of contours extracted from Mitchell et al. (2012) constitute interpolation artefacts.

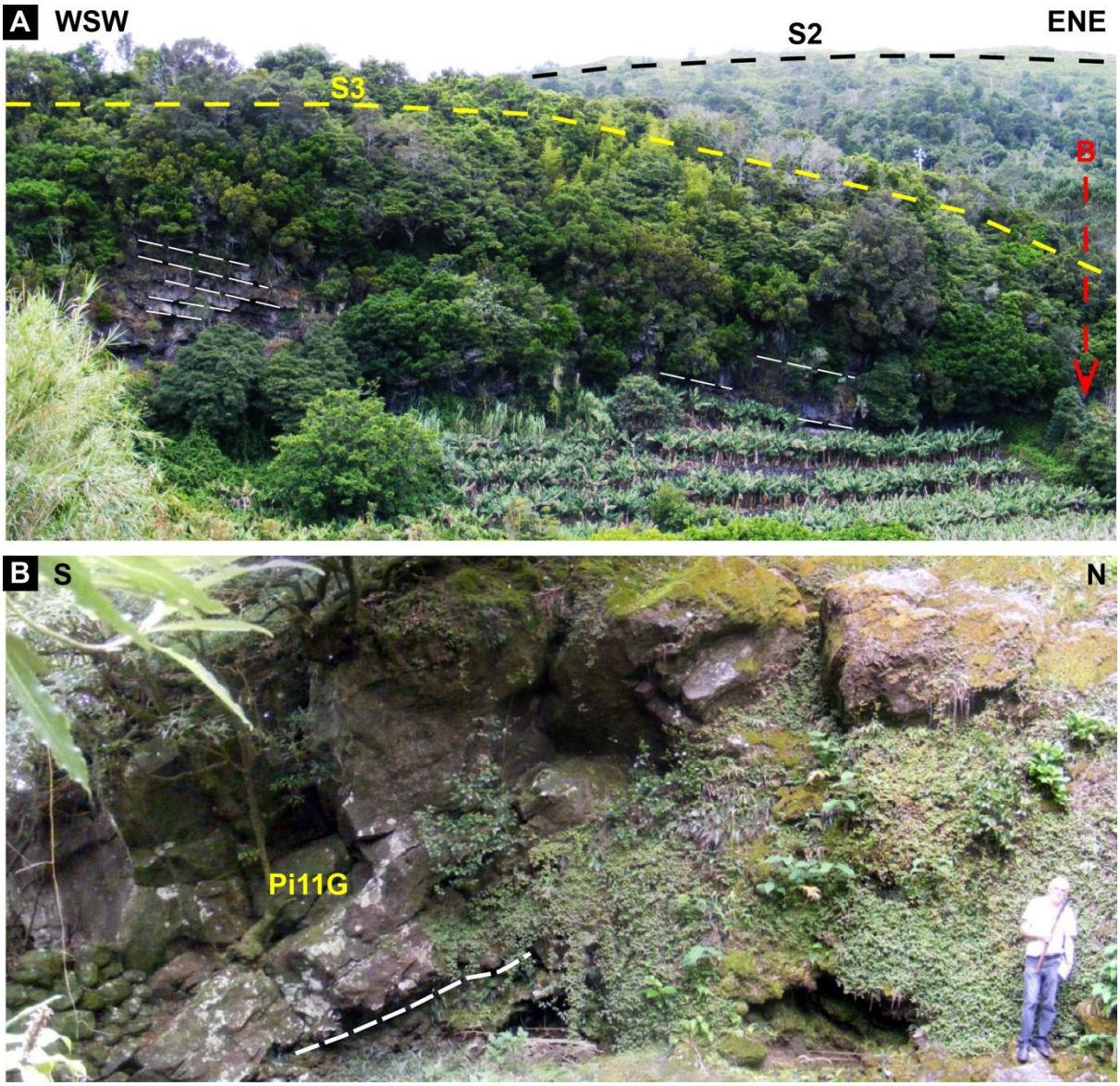

Fig. A.8. (A) View of the easternmost sector of S3. The outcropping sequence locally apparently dips towards E. **(B)** Location of sampling of Pi11G. The lava flow is laterally continuous to the sequence visible on (A).

References

Afonso, A., Gomes, F., Fernandes,M., 2002. IGeoE: Cartografia de qualidade - a base de um SIG. Trib. das Autarquias 108, 13–14 (Jun. 2002).

Costa, A.C.G., Marques, F.O., Hildenbrand, A., Sibrant, A.L.R., Catita, C.M.S., 2014. Large-scale catastrophic flank collapses in a steep volcanic ridge: The Pico–Faial Ridge, Azores Triple Junction. J. Volcanol. Geotherm. Res. 272, 111-125, http://dx.doi.org/10.1016/j.jvolgeores.2014.01.002.

Hildenbrand, A., Marques, F.O., Catalão, J., Catita, C.M.S., Costa, A.C.G., 2012a. Large-scale active slump of the southeastern flank of Pico Island, Azores. Geology 40 (10), 939–942. http://dx.doi.org/10.1130/G33303.1.

Kongsberg, S., 2007. EM 120 Multibeam Echo Sounder, Product Description. Kongsberg Maritime AS, Norway, Bremerhaven, Pangaea 44 p. (available at http://epic.awi.de/26725/1/Kon2007a.pdf).

Lourenço, N., Miranda, J.M., Luis, J.F., Ribeiro, A., Mendes Victor, L.A., Madeira, J., Needham, H.D., 1998. Morpho-tectonic analysis of the Azores Volcanic Plateau from a new bathymetric compilation of the area. Mar. Geophys. Res. 20 (3), 141-156. http://dx.doi.org/10.1023/A%3A1004505401547.

Mitchell, N.C., Quartau, R., Madeira, J., 2012. Assessing landslide movements in volcanic islands using near-shore marine geophysical data: south Pico Island, Azores. Bull. Volcanol. 74 (2), 483–496. http://dx.doi.org/10.1007/s00445-011-0541-5.